Chapter 10

Cloud Microphysical Properties, Processes, and Rainfall Estimation Opportunities

DANIEL ROSENFELD

Institute of Earth Sciences, Hebrew University of Jerusalum, Jerusalem, Israel

CARLTON W. ULBRICH

Department of Physics and Astronomy, Clemson University, Clemson, South Carolina

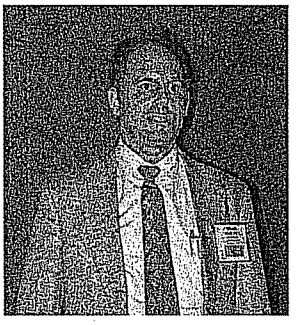

Rosenfeld

1. Introduction

In this work the longstanding question of the connections between raindrop-size distributions (RDSDs) and radar reflectivity–rainfall rate (Z–R) relationships is revisited, this time from the combined approach of rain-forming physical processes that shape the RDSD, and a formulation of the RDSD into the simplest free parameters of the rain intensity R, rainwater content W, and median volume drop diameter D_0. This is accomplished through a theoretical analysis, using a gamma RDSD, of D_0–R and W–R relations implied by the coefficients and exponents in empirical Z–R relations. The results provide a means by which these Z–R relations can be classified. The most dramatic of these classifications involves the relation between D_0 and W, which shows a remarkable ordering with the rain types.

This work also summarizes the effects of various physical processes in modifying the RDSD in clouds. These individual processes are combined into conceptual models of the way different microphysical and dynamical rain-forming processes can build different kinds of RDSDs. Much of the physical insights that are at the heart of this study came from examining the evolution of the RDSD with respect to its ultimate mature state of the equilibrium raindrop-size distribution described by Hu and Srivastava (1995).

Finally, the different components of the previous sections are combined in an examination of integral parameters deduced from the raindrop-size distributions associated with the host of RDSD-based Z–R relations found in the literature. Only those relations are used that could be associated to the cloud microstructure and dynamic context of the conceptual model. It is found that there exists a well-defined sequence in the transition from extreme continental to equatorial maritime for convective rainfall. In addition, similar behavior is found in tropical convective versus stratiform rainfall and in orographic rainfall as a function of altitude. These results offer promise for the development of algorithms for classification of the rainfall with respect to type in the remote measurement of rainfall either from satellite platforms or from ground-based radars.

Early attempts to explain the variability in Z–R relations are reviewed in section 2. Section 3 reviews the formulation of the RDSD and provides the tools to restore RDSD parameters from published Z–R power-law relations. Section 4 describes the way the different individual processes that modify the RDSD can be combined into conceptual models of the rain-forming pro-

TABLE 10.1. Microphysical and kinematic influences on Z–R relationships and the effect on radar rainfall estimates when no adjustment is applied (after Wilson and Brandes 1979).

Process	Change in $Z = AR^b$		Probable effect on radar rainfall if Z–R not adjusted	Possible region of max influence
	A	b		
Microphysical				
Evaporation (Atlas and Chmela 1957)	Increase	Decrease	Overestimate	Inflow regions, fringe areas
Accretion of cloud particles (Atlas and Chmela 1957; Rigby et al. 1954)	Decrease	Increase	Underestimate	Downdraft
Collision, coalescence (Srivastava 1971)	Increase	Decrease	Overestimate	Reflectivity core
Breakup (Srivastava 1971)	Decrease	Decrase	Underestimate	Reflectivity core
Kinematic				
Size sorting (Gunn and Marshall 1955; Atlas and Chmela 1957)	Increase	Decrease	Tendency to overestimate	Regions of strong inflow and outflow
Vertical motion				
Updraft	Increase	Decrease	Overestimate	
Downdraft	Decrease	Increase	Underestimate	

cesses. Section 5 applies the different components in the previous sections to deduce the Z–R classification scheme. Section 6 summarizes the results and offers suggestions for implementation of a dynamic Z–R classification method.

2. Early attempts to classify Z–R relations

It has long been recognized that wide range of values found for the coefficient A and exponent b in Z–R relations of the form $Z = AR^b$ is due to variations in the form of the RDSD. Chandrasekar et al. recognize this connection between RDSD variability and the values of A and b (chapter 9 in this monograph). They also point to the importance of separating Z–R relations according to the type of rainfall. One of the earliest studies to recognize these effects was that due to Atlas and Chmela (1957) who showed that RDSD sorting at the scale of the individual rain shaft could occur due to drop sorting by wind shear and updrafts. Beyond the scale of the individual rain shafts, the causes of variability in Z–R relations were sought in differences in rainfall types, atmospheric conditions, and geographical locations (Fujiwara 1965; Stout and Mueller 1968; Cataneo and Stout 1968). The rationale was that different conditions would prefer different rain processes, and the effects of these processes were summarized in the form of a table in Wilson and Brandes (1979), which is reproduced here as Table 10.1.

Wilson and Brandes (1979) provided this table with little discussion. Such a discussion is provided later in this work, with some explanations on the causes for the trends of the coefficient and exponent. That is done after the various analytical forms of the RDSD that have been employed in the past are introduced.

To depict the relationships between the various parameters of the RDSD, Atlas and Chmela (1957) produced a rain parameter diagram (RAPAD) with Z plotted versus R and on which isopleths of distribution parameters were displayed for an exponential distribution of the form

$$N(D) = N_0 \exp(-\Lambda D), \qquad (10.1)$$

where $N(D)$ (m^{-3} cm^{-1}) is the number of drops per unit volume per unit size interval and N_0 and Λ are the RDSD parameters. In addition, as shown by Atlas (1955), $\Lambda = 3.67/D_0$, where D_0 is the median volume diameter. The Atlas–Chmela diagram is reproduced in Atlas (1964), but a more recent version is shown in Fig. 10.1 for an exponential distribution with isopleths of W, D_0, and N_0, where W(g m^{-3}) is the liquid rainwater concentration. At the time the Atlas–Chmela diagram was published, the use of Z (the single radar measurable then available) to measure R through the use of a Z–R relation was the focus of research in radar meteorology. As the field expanded the number of measurements of drop-size spectra (and Z–R relations derived from them) grew rapidly and it was discovered quickly that there was no unique relationship between Z and R; that is, there were no unique values for A and b. The advantage of the Atlas–Chmela Z–R rain parameter diagram was that for a given Z–R relation (*and* an exponential RDSD), it permitted the relationships between all of the drop-size distribution (DSD) integral parameters to be determined. That is, for a given Z–R relation the diagram implied corresponding relations between D_0–R, W–R, Z–W, D_0–W, etc.. The disadvantage was that a different diagram had to be produced for distributions different from exponential.

There have been many attempts to relate the large observed variations in the coefficient A and exponent b in the Z–R law to the meteorological conditions associated with the rainfall and to the parameters of the drop-size distribution. It is well known in radar meteorology that there is a great lack of consistency in the drop-size distribution for various meteorological conditions. Even when the conditions appear to be similar the size distributions can be widely different. This is apparent in

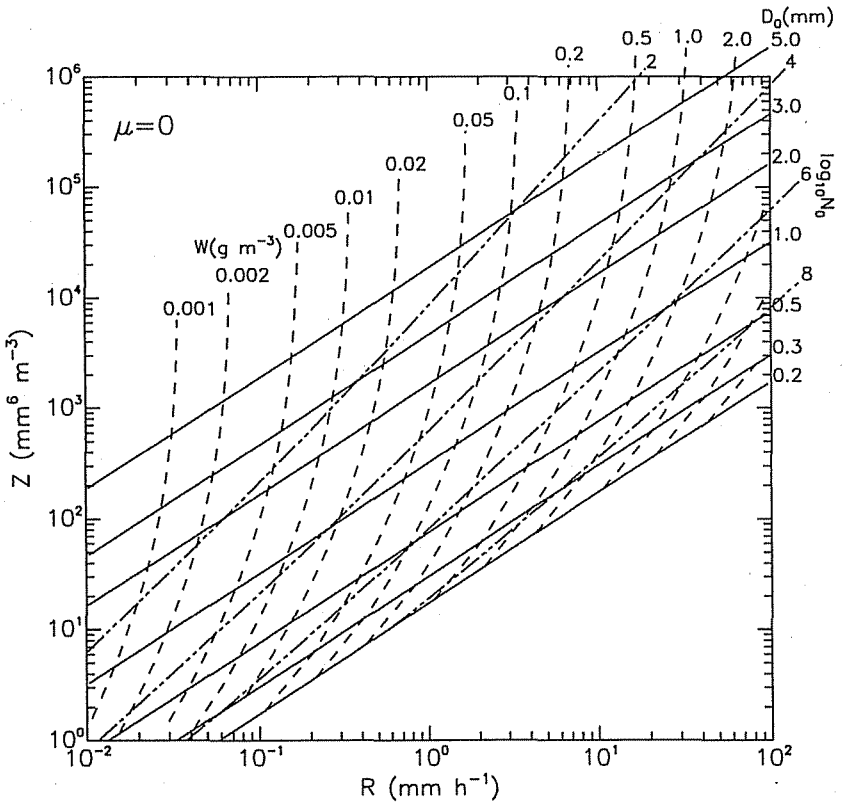

FIG. 10.1. Rain parameter diagram of Ulbrich and Atlas (1978) similar to that presented by Atlas and Chmela (1957) for an exponential RDSD. The solid, dashed, and dash–double-dotted lines are isopleths of median volume diameter D_0, liquid water concentration W, and exponential intercept parameter N_0. The isopleths are labeled with the values to which they correspond with the units of mm for D_0, g m^{-3} for W, and m^{-3} cm^{-1} for N_0.

the work of Fujiwara (1965) who uses results for A and b derived from analysis of data collected at the surface with a raindrop camera (Mueller 1965) together with radar data and National Weather Service reports to deduce those regions on a plot of A versus b, which correspond to a given rainfall type. Data were analyzed for four locations, namely, Florida, Illinois, Germany, and Japan. Fujiwara considers only three types of rainfall, that is, thunderstorms, showers, and continuous rain and, although there is much scatter on the A–b plot, he enumerates some general findings. He finds that large A (300–1000) and moderate b (1.25–1.65) are associated with thunderstorms, while both A and b are somewhat smaller and more variable for rain showers. For continuous rain the values of A are generally smaller than for either of the previous two types, but the range of b is large (1.0–2.0). The results found for thunderstorms in Illinois are in essential agreement with those found for the Florida data. He also attempts to relate A and b to the shapes of the drop-size distribution and to the characteristics of the radar echo. The distributions for thunderstorm rain were found to tend toward exponentiality with drops of large diameters and several peaks. For weak rain showers the distribution is sharply peaked at small diameters and concave downward on a plot of $\log[N(D)]$ versus D. However, all drop-size distributions in Fujiwara's analysis are concave downward and exhibit considerable shortage of drops with diameters less than about 1 mm. This may be due to an inability of the drop camera to detect these drops and thus precludes definitive conclusions about the dependence of A and b on RDSD shape. In any event, the absence of small drops has little effect on the values of Z and R and, hence, on the values of A and b. For the three types of rainfall Fujiwara finds central values of $(A, b) = (450, 1.46)$ for thunderstorms, (300, 1.37) for rain showers, and (205, 1.48) for continuous rain. There is a great deal of scatter in Fujiwara's results for A and b when plotted on an A versus b diagram, but there is a weak suggestion of an inverse dependence of A on b; that is, large A corresponds to small b, etc.

Similar work of this nature has been conducted by investigators at the Illinois State Water Survey using data from the same instrument as that used by Fujiwara. Stout and Mueller (1968) report measurements from Florida, the Marshall Islands, and Oregon and classify their Z–R relations separately according to rainfall type (continuous, showers, or thunderstorms), synoptic situation (air mass, warm front, cold front, etc.), and thermodynamic instability. The results of classification by

TABLE 10.2. Values of A and b in $Z = AR^b$ for tropical stratiform and convective rainfall in TOGA COARE.

Source	Stratiform		Convective	
	A	b	A	b
Tokay et al. (1995)	335	1.37	175	1.37
Tokay and Short (1996)	367	1.30	139	1.43
Atlas et al. (2000)	224	1.28	129	1.38
Ulbrich and Atlas (2002)	203	1.46	120	1.43

thermodynamic instability were found not to be useful, but those found from the classification by rainfall type and synoptic situation displayed large systematic variations in A and b, indicating the importance of using a stratification technique for measurement of rainfall using Z–R relations. In spite of this finding, neither of the first two techniques was found to be superior in measuring rainfall amounts to the method that uses the Z–R relation given by Marshall et al. (1947). In fact, in several cases the latter was found to produce more accurate results than either stratification method.

Some limited progress in this area has been made recently for tropical rainfall. Well-defined differences in stratiform and convective rainfall in the Tropics have been found by several investigators during Tropical Oceans Global Atmosphere Coupled Ocean–Atmosphere Response Experiment (TOGA COARE). Some of the results found for A and b by various investigators are listed in Table 10.2. It must be recognized that these relations are based on long-term temporal and spatial averages of experimental RDSDs. For individual storms and for stages of such storms the Z–R relations can vary appreciably. For example, Atlas et al. (1999) show data for tropical squall lines that are segmented into convective (C), transition (T), and stratiform (S) stages. The variations in A and b between different storms for each of these stages are very large and can also vary appreciably between storms. In any event, it is clear from Table 10.2 that there is not much difference between these relations for convective rain when plotted on the rain parameter diagram of Atlas and Chmela (1957; Fig. 10.1). The differences between the stratiform relations lie mostly in the coefficients, which Atlas et al. (2000) attribute to the inclusion by Tokay and Short (1996) of transition rain in the convective category. Nevertheless, it may be concluded from the results shown above that the principal differences between stratiform and convective rain in the Tropics is that the coefficient A for stratiform rain is somewhat larger (at least 70%) than the coefficient for convective rain. Examination of these relations, when plotted on the RAPAD of Fig. 10.1, indicates that the larger coefficients A for stratiform rain are associated with larger Z values (for the same R) than convective rain and therefore also with larger values of D_0.

3. Formulations of the raindrop-size distribution

Raindrop-size distributions have been a subject of extensive investigation for nearly 100 years. The earliest carefully performed measurements of raindrop sizes were reported by Laws and Parsons (1943), Marshall and Palmer (1948), and Best (1950) and indicated that the distribution could be approximated well by an exponential function of the form of Eq. (10.1). (In the following the term "raindrop size" is used to mean raindrop diameter). This mathematical approximation to the raindrop-size distribution has been in widespread use for decades and is especially convenient because of its simplicity. However, even in the early experimental work just cited distinct deviations from exponentiality were noted. Since these deviations are reflective of the physics of rain formation in clouds it has been considered imperative that an accurate mathematical representation of the distribution be found.

To account for distribution shape effects Atlas (1955) introduced a "moment" G of the distribution, which related the reflectivity factor Z to the median volume diameter D_0 and the liquid water concentration M. They also showed Z to be related to the rainfall rate R and D_0 through the moment G. Joss and Gori (1978) also defined measures of distribution shape $S(PQ)$, where P and Q are any two integral parameters of the distribution. For distributions that have breadth narrower than, equal to, or broader than an exponential distribution, S is less than, equal to, or greater than 1, respectively. For the experimental distributions they investigate, Joss and Gori find that S is always less than 1, the more so the shorter the time interval used to average the data. Joss and Gori also found that considerable long-term averaging of disdrometer data is required for the distributions to approach exponentiality; the longer the averaging period the closer the approach to exponentiality. Periods as long as 256 min were required to find average distributions close to exponential, regardless of the type of rainfall. Their work further demonstrates the need for RDSDs of greater generality than the exponential distribution.

Other attempts to account for distribution shape have involved the use of specific mathematical forms different from exponential. One of the earliest of these was a lognormal function suggested by Levin (1954) of the form

$$N(D) = N_0 D^{-1} \exp(-c \ln^2[D/D_g]), \qquad (10.2)$$

with N_0, c, and D_g as parameters. This form has been applied to the analysis of cloud droplet and raindrop distributions by many investigators including Mueller and Sims (1966), Bradley and Stow (1974), and Markowitz (1976). Although this function approximates drop-size distributions well, it does not allow for as broad a spectrum of RDSD shapes as other representations and does not reduce to the exponential function as a special case. An alternative function that has come

into widespread use is the gamma function having the form

$$N(D) = N_0 D^{\mu} \exp(-\Lambda D), \quad (10.3)$$

with N_0, μ, and Λ as parameters (Deirmendjian 1969; Willis 1984; Ulbrich 1983). The advantages of this distribution are that it reduces to the exponential distribution when $\mu = 0$ and it allows for distributions with a wide variety of shapes including those that are either concave upward or downward on a plot of $\log[N(D)]$ versus D. RDSD shapes of this type are very apparent in experimental spectra collected at the earth's surface using various sampling devices, such as drop cameras, disdrometers, 2D optical probes, and video recorders. An early example of an investigation that displays these effects is that of Dingle and Hardy (1962). More recent examples are very prevalent; one that includes extensive analysis of tropical raindrop spectra is that of Tokay and Short (1996). Such data usually consist of samples of short duration (e.g., 1 min). However, Levin et al. (1991) find such effects in disdrometer data even when averaged for periods as long as 2 h. It might also be stated that these effects may not be representative of RDSD shapes observed aloft with radar. However, shape effects similar to that found with surface instruments also exist in RDSDs aloft as is apparent from the early work of Rogers and Pilié (1962) and Caton (1966), who acquired Doppler radar spectra of rain at vertical incidence. They are also apparent in the analysis by Atlas et al. (2000) of 2D optical probe data acquired aloft during TOGA COARE by an National Center for Atmospheric Research (NCAR) *Electra* aircraft. The gamma distribution has properties that provide an accurate representation to be made of these shape effects. In addition, integral rainfall parameters generally are simple to calculate with the gamma distribution.

In spite of its advantages there are features that make this function troublesome. First, the coefficient N_0 no longer has the simple units as the equivalent coefficient in the exponential distribution and, in fact, includes the parameter μ. As a result N_0 and μ are strongly correlated as shown by Ulbrich (1983), but this correlation is demonstrated by Chandrasekar and Bringi (1987) not to imply any physical basis. To avoid this problem they rewrite the distribution in the form

$$N(D) = \frac{N_T}{\Gamma(\mu + 1)\Lambda^{\mu+1}} D^{\mu} \exp(-\Lambda D), \quad (10.4)$$

where N_T is the total concentration of raindrops, and recommend using N_T, μ, and Λ as the distribution parameters. Note that N_T can be written as

$$N_T = N_0 \Gamma(\mu + 1)/\Lambda^{\mu+1} \quad (10.5)$$

so that this form requires that $\mu > -1$. Values of $\mu \leq -1$ will produce results for N_T that are undefined. Willis (1984) normalized the distribution so that it assumed the form

$$N(D) = N_G (D/D_0)^{\mu} \exp(-\Lambda D/D_0), \quad (10.6)$$

where the coefficient N_G is expressed in terms of the liquid water concentration W by

$$N_G = (6W\Lambda^{4+\mu})/(\pi\, \Gamma(4 + \mu)). \quad (10.7)$$

In similar fashion, Testud et al. (2001) normalized the gamma distribution using W and the mean volume diameter D_m by writing it as

$$N(D) = N_0^* F_{\mu}(X), \quad (10.8)$$

where $X = D/D_m$, $N_0^* = 4^4 W/(\pi D_m^4)$,

$$F_{\mu}(X) = C_{\mu} X^{\mu} \exp(-(4 + \mu)X), \quad (10.9)$$

and $C_{\mu} = (\Gamma(4)(4 + \mu)^{4+\mu})/(\Gamma(4 + \mu)4^4)$. As long as values of N_T are not required, the latter two normalizations will yield useful results for $\mu > -3$.

Another analytical expression for the drop-size distribution that represents some types of experimental drop-size data fairly well is that of Imai (1964). It may be written

$$N(D) = 6\sqrt{\frac{h}{\pi^3}} W D^{-3} \exp[-h(D - D_0)^2], \quad (10.10)$$

where W is the liquid water concentration, D_0 is the median volume diameter, and h is a parameter. The distribution may be easily normalized such that it has the form

$$N^*(D) = C\Delta^{-3} \exp(-(\Delta - \Delta_0)^2), \quad (10.11)$$

where $C = (6h^3 W)/\pi^{3/2}$ and $\Delta = \sqrt{h} D$. For $\sqrt{h} D_0 > \sqrt{6}$ the normalized curves show one maximum and one minimum and for $\sqrt{h} D_0 < \sqrt{6}$ the curves show no extrema but one inflection point. The form of the DSD with $\sqrt{h} D_0 < \sqrt{6}$ is similar to that displayed by the experimental data of Marshall and Palmer (1948), whereas the form for $\sqrt{h} D_0 > \sqrt{6}$ is similar to that of the equilibrium distributions of Hu and Srivastava (1995). The disadvantage of this distribution is that it implies that the mass is distributed normally with respect to diameter.

None of these "normalization" methods removes the strong correlation among the DSD parameters that is commonly observed in experimental data. These parameters cannot, therefore, be considered strictly independent, a property of distribution parameters that is highly desirable in remote sensing algorithms. In an investigation of methods to avoid this problem, Haddad et al. (1996) found parameters of the gamma distribution that are negligibly correlated and may therefore be considered independent. One of these is chosen to be the rainfall rate R and the other two, D' and s', are defined in terms of R, D_m (the mean volume diameter), and s_m (the relative standard deviation of the mass spectrum) as

$$D' = D_m R^{-0.155} \quad \text{and} \quad (10.12)$$

$$s' = s_m D_m^{-0.2} R^{0.031} \exp(0.017 R^{0.74}). \quad (10.13)$$

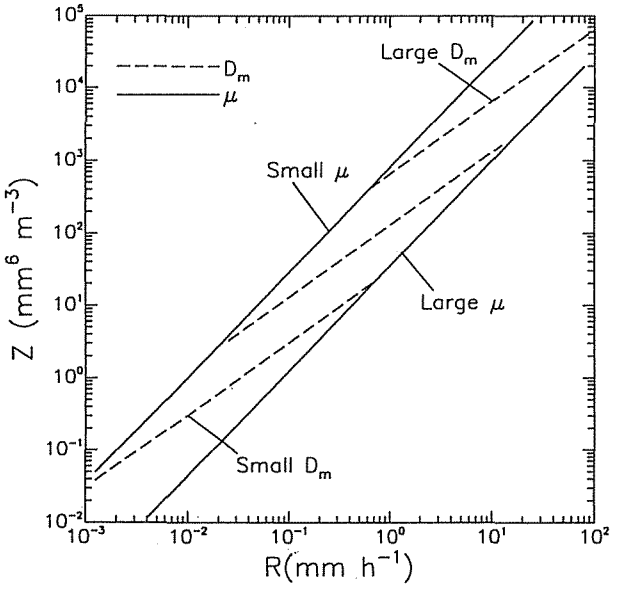

FIG. 10.2. The simplified rain parameter diagram for a gamma RDSD from Ulbrich and Atlas (1998). The solid lines are isopleths of the gamma distribution shape parameter μ, and the dashed lines are isopleths of the mean volume diameter D_m. The μ isopleths have slopes equal to that of the Z–R relation that applies to the dataset under consideration.

The values of the coefficients and exponents in these expressions were determined for a set of raindrop-size distribution data acquired by a Joss disdrometer near Darwin, Australia, in the summers of 1988/89 and 1989/90. It remains to be demonstrated that these expressions apply to raindrop distributions in general.

Ulbrich and Atlas (1998) have shown a version of the rain parameter diagram that employs the gamma RDSD and, as in the Atlas–Chmela diagram, consists of a logarithmic plot of Z versus R but with isopleths of μ and D_m (the mean volume diameter) for a gamma distribution. It is shown in Fig. 10.2. The μ isopleths are parallel to the Z–R relation, which applies to the dataset of interest, and the D_m isopleths have slopes equal to 1. For a set of experimental Z–R data, the diagram shows how the shape μ and breadth D_m vary within the dataset. It does not require the assumption of a specific distribution shape but does require knowledge of the empirical Z–R relation for the dataset in question.

Although all of the analytical expressions given above provide useful and usually accurate approximations to most observed drop-size distributions, not all experimental distributions behave as smoothly as these functions. When such behavior is evident it is difficult, perhaps impossible, to describe the distribution accurately using mathematical formulas similar to those given above. An example may be found in the work of Steiner and Waldvogel (1987) who found multiple distribution peaks at raindrop diameters of approximately 0.7, 1.0, 1.9, and (perhaps) 3.2 mm. Similar measurements by de Beauville et al. (1988) in a maritime tropical environment find peaks at 0.6, 1.0, 1.8, and 3 mm. Each of these investigations support the predictions of earlier theoretical work by several investigators who predict trimodal distributions in equilibrium rainfall, that is, rainfall in which the actions of collisional breakup and coalescence produce equilibrium size distributions. Examples of such calculations are found in the work of Valdez and Young (1985), List et al. (1987), Hu and Srivastava (1995), and Brown (1989). Hu and Srivastava (1995) also find that when evaporation is included an approximate equilibrium RDSD is still possible. Valdez and Young (1985) find peaks at 0.268, 0.79, and 1.76 mm; List et al. (1987) find them at 0.24, 0.87, and 2.0 mm; and Hu and Srivastava (1995) determine peaks to be at 0.2, 0.9, and 1.5 mm. None of the experimental work has been able to resolve diameters as small as the first of these peaks, but the second and third are very similar to the experimentally determined values. Disagreements between the experimental and theoretical values may be due to insufficient time for the observed clouds to reach an equilibrium situation. For example, the clouds observed by de Beauville et al. (1988) were all showers of duration less than 10 min. In spite of the peakedness of these spectra, Steiner and Waldvogel (1987) show that they have little influence on Z–R relations used in the remote measurement of rainfall. Integral parameters such as Z and R are not affected very much by the presence of these peaks in the distribution so that one may have confidence that the analytical approximations described above will be adequate representations of the actual distribution except for the finescale details.

Some of the earliest work on equilibrium distributions was done by Srivastava (1971), who considered the evolution of drop-size distributions under the action of drop coalescence and spontaneous breakup. He found computed distributions with considerable shape tending toward downward concavity but with numbers of small diameter drops greater than could be described by a downward concave gamma distribution. The important characteristic feature of the distributions corresponding to different rainfall rates was that they were essentially parallel to one another. In other words, the distributions corresponding to different rainfall rates were all multiples of one another. This result has also been found by Donaldson (1984) and List et al. (1987) using a similar theoretical model that includes drop breakup and coalescence. List (1988) therefore writes the equilibrium distribution as a product of the rainfall rate R and a shape function, that is,

$$f_N(D, R) = R\psi_N(D), \tag{10.14}$$

which means that all integral rainfall parameters can be written as the product of a constant and the rainfall rate. For example, the total number concentration is $N_T = C_N R$, the liquid water concentration is $W = C_M R$, the reflectivity factor is $Z = C_Z R$, etc., where C_N, C_M, and

TABLE 10.3. Definitions of various raindrop integral parameters.

Symbol	Parameter	p	a_P
Z	Reflectivity factor	6	10^6 mm^6 cm^{-6}
W	Liquid water concentration	3	0.524 g cm^{-3}
R	Rainfall rate	3.67	33.31 mm h^{-1} m^3 cm$^{-3.67}$
N_T	Total number concentration	0	1.0

C_Z are constants. Note that the latter relation implies that in equilibrium rainfall a linear relation exists between Z and R. Atlas and Ulbrich (2000) show that a direct proportionality between Z and R also implies that the median volume diameter D_0 must be constant in time during the rainfall event. Although this behavior has been observed infrequently in nature with surface disdrometer data, Atlas and Ulbrich (2000) show spectra acquired aloft for storms in TOGA COARE for which the constancy of D_0 and proportionality of Z and R are evident. These spectra closely resemble the equilibrium spectra of List et al. (1987) and Hu and Srivastava (1995) and display a tendency for a peak occurring near a diameter of 1.5 mm, in agreement with the theoretical predictions.

In this work the gamma RDSD will be employed to deduce the behavior of integral parameters implied by the values of the coefficient A and exponent b in the Z–R law. This is done in the manner described by Ulbrich (1983), which uses A and b to compute the gamma distribution parameters and proceeds in the following way. Any integral parameter P may be expressed in terms of the gamma distribution as

$$P = a_P \int_0^\infty D^p N(D)\, dD = a_P \frac{\Gamma(p + \mu + 1)}{(3.67 + \mu)^{p+\mu+1}} N_0 D_0^{p+\mu+1}. \quad (10.15)$$

Note that the method assumes $D_{\min} = 0$, $D_{\max} \to \infty$. The effects on integral parameters and empirical relations of assuming values for $D_{\min}$ and $D_{\max}$ different from these values have been investigated by Ulbrich (1985, 1992, 1993). For parameters Z, W, R, and N_T the values of p and a_p are listed in Table 10.3.

In the above it has been assumed that the fall speeds of the drops in still air are given by a power law in terms of the diameter as given by Atlas and Ulbrich (1977), that is,

$$v(D) = 17.67 D^{0.67}, \quad (10.16)$$

where $v(D)$ is in meters per second and D is in centimeters. This is a good approximation to the raindrop fall speeds at sea level and is sufficiently accurate for the present purposes.

Consider a pair of integral parameters P and Q. The theoretical expression for Q is the same as that shown above for P with a_Q and q substituted for a_p and p, respectively:

$$Q = a_Q \int_0^\infty D^q N(D)\, dD = a_Q \frac{\Gamma(q + \mu + 1)}{(3.67 + \mu)^{q+\mu+1}} N_0 D_0^{q+\mu+1}. \quad (10.17)$$

Elimination of D_0 between P and Q results in the form

$$P = \alpha Q^\beta, \quad (10.18)$$

where

$$\beta = \frac{p + \mu + 1}{q + \mu + 1} \quad \text{and} \quad (10.19)$$

$$\alpha = \frac{a_P \Gamma(p + \mu + 1) N_0^{1-\beta}}{[a_Q \Gamma(q + \mu + 1)]^\beta}. \quad (10.20)$$

These equations can be inverted to obtain expressions for μ and N_0, that is,

$$\mu = \frac{p - \beta q}{\beta - 1} - 1 \quad \text{and} \quad (10.21)$$

$$N_0 = \left\{ \frac{\alpha \left[a_Q \Gamma\left(\frac{p - q}{\beta - 1} \right) \right]^\beta}{a_P \Gamma\left[\frac{\beta(p - q)}{\beta - 1} \right]} \right\}^{1/(1-\beta)}. \quad (10.22)$$

This approach assumes that the parameter N_0 is constant or at least slowly varying with R. In this work we consider the examples of P–Q relations of the form $Z = AR^b$, $D_0 = \epsilon R^\delta$, $N_T = \xi R^\eta$ and $W = \zeta R^\kappa$. The coefficient A and exponent b in an empirical Z–R relation are used to find μ and N_0 from which the coefficients and exponents for the remaining three relations are calculated. The coefficients and exponents for all these relations are listed in the Table 10.4.

TABLE 10.4. Relations between integral rainfall parameters found from Eqs. (10.18)–(10.20) assuming a gamma RDSD.

P–Q relation	Coefficient	Exponent
$Z = AR^b$	$A = \dfrac{10^6 \Gamma(7 + \mu) N_0^{-2.33/(4.67+\mu)}}{[33.31 \Gamma(4.67 + 1)]^{(7+\mu)/(4.67+\mu)}}$	$b = \dfrac{7 + \mu}{4.67 + \mu}$
$D_0 = \varepsilon R^\delta$	$\varepsilon = \dfrac{3.67 + \mu}{[33.31 N_0 \Gamma(4.67 + 1)]^{1/(4.67+\mu)}}$	$\delta = \dfrac{1}{4.67 + \mu}$
$N_T = \xi R^\eta$	$\xi = \dfrac{\Gamma(1 + \mu) N_0^{3.67/(4.67+\mu)}}{[33.31 \Gamma(4.67 + \mu)]^{(1+\mu)/(4.67+\mu)}}$	$\eta = \dfrac{1 + \mu}{4.67 + \mu}$
$W = \zeta R^\kappa$	$\zeta = \dfrac{\pi \Gamma(4 + \mu) N_0^{0.67/(4.67+\mu)}}{6[33.31 \Gamma(4.67 + \mu)]^{(4+\mu)/(4.67+\mu)}}$	$\kappa = \dfrac{4 + \mu}{4.67 + \mu}$

The corresponding expressions for N_0 and μ in terms of A and b are

$$N_0 = \left\{ \frac{A\left[33.31\Gamma\left(\frac{2.33}{b-1}\right)\right]^b}{10^6\Gamma\left(\frac{2.33b}{b-1}\right)} \right\}^{1/(1-b)} \quad \text{and} \quad (10.23)$$

$$\mu = \frac{7 - 4.67b}{b - 1}. \quad (10.24)$$

It should be noted that there are a couple of instances in which this approach will not yield useful results. First of all, if $\mu \leq -1$, then N_T is undefined. Second, if b is very close to 1 (as in the case of the equilibrium drop-size distribution), then μ becomes very large. In neither of these cases are the results found for the coefficients and exponents in the above table considered to be physically meaningful.

These results may now be used to illustrate the effects on the coefficient A and exponent b of each of the various physical process listed in Table 10.1. For the purposes of illustration the RDSD before modification is shown as an exponential distribution on most of the diagrams that follow and is represented by a straight line. However, it is clear that the RDSD could have any shape before modification. In describing the changes that take place, the equation for N_T in terms of N_0, μ, and D_0 is used. From Eq. (10.15) the expression for N_T may be shown to have the form

$$N_T = \frac{N_0 D_0^{1+\mu}\Gamma(1 + \mu)}{(3.67 + \mu)^{1+\mu}}. \quad (10.25)$$

Wilson and Brandes (1979) provided qualitative microphysical and kinematic influences on Z–R relationships, presented in Table 10.1. Here, with the added benefit of the additional RDSD formulations, this can be expanded and tie the different physical processes to the parameters presented in Table 10.3 and the Z–R relation parameters. The discussion is presented for each factor acting alone, assuming everything else is held constant. Admittedly, it is rarely the case in reality; however, it serves the purpose of understanding the various processes that combine to form the actual RDSDs.

a. Coalescence (Fig. 10.3a)

Modification of the RDSD by coalescence alone decreases the numbers of small diameter drops and increases those of the larger drops. Consequently, D_0 must increase and the total number concentration of drops N_T must decrease. The process also increases μ; the amount by which it would change depends on the efficiency of the coalescence process. The result is a decrease in N_0 and a consequent increase in A and small decrease in b. There would be an approximate parallel shift in the Z–R relation on the RAPAD upward and to the left, perpendicular to the D_0 isopleths. It would be necessary

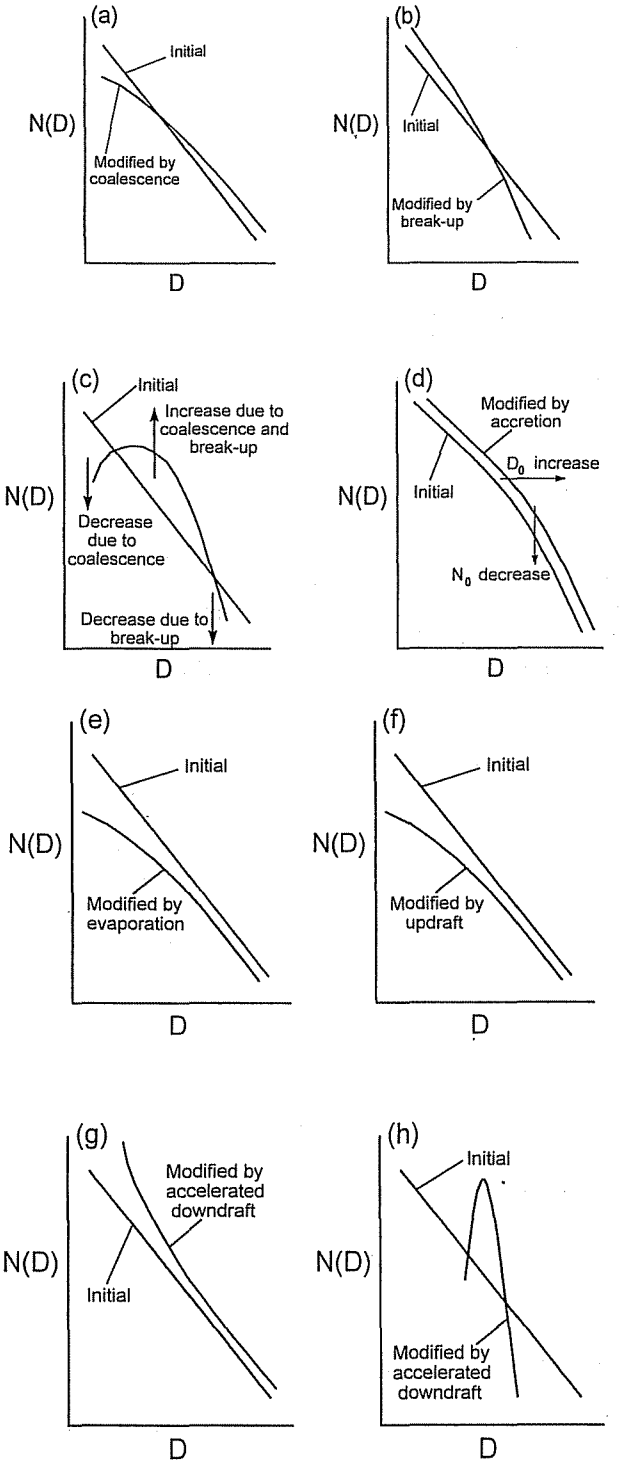

FIG. 10.3. Schematic depictions of the effects of various processes on the shape of the RDSD. The processes illustrated are (a) raindrop coalescence, (b) raindrop breakup, (c) coalescence and breakup acting simultaneously, (d) accretion of cloud droplets, (e) evaporation, (f) an updraft, (g) an accelerated downdraft, and (h) size sorting.

to use a RAPAD for a different value of μ before and after modification.

b. Breakup (Fig. 10.3b)

Modification of the RDSD by breakup alone increases the numbers of small diameter drops and decreases the numbers of large diameter drops. There must be a consequent decrease in D_0 and an increase in N_T. Accordingly, N_0 must increase. There is probably a small change in μ with a tendency toward a decrease. The end result is a decrease in A and a small increase (or perhaps no change) in b. Because of the small change in μ we may use the same RAPAD before and after modification. There is therefore an approximate shift in the Z–R relation on the RAPAD downward and to the right, approximately parallel to the D_0 isopleths.

c. Coalescence and breakup combined (Fig. 10.3c)

Breakup is more important at the larger sizes, coalescence more important at small sizes (insofar as numbers are concerned). Both processes acting together increase μ substantially. The degree to which μ changes depends on the relative strengths of the two processes in real cloud situations. This requires using a different RAPAD before and after modification; that is, the isopleths will shift. The apparent increase in μ will decrease b. What will happen to A depends on which of the two processes is predominant.

d. Accretion (Fig. 10.3d)

Since accretion of cloud particles by raindrops acts to increase the sizes of all particles without increasing their numbers, then N_T must remain unchanged. If all drops grow at the same rate, this implies a shift of the RDSD parallel to itself to larger diameters with a consequent increase in D_0. Since N_T remains constant, N_0 must decrease. The result is an increase in A and probably little change in b. Since μ is unchanged, the same RAPAD before and after modification can be used. Therefore, the Z–R law will be shifted parallel to itself upward on the RAPAD. In reality, larger raindrops have greater terminal velocity and therefore have larger growth rate by accretion. When also adding to consideration the creation of new small drops, the process mirrors the effect of evaporation, as discussed next.

e. Evaporation (Fig. 10.3e)

The presence of evaporation acting alone will result in a greater loss of the numbers of small diameter particles than large drops. Consequently, N_T is not constant and must decrease. There must also be a substantial change in the shape of the RDSD so that μ increases. Also, D_0 must increase. The result is a decrease in N_0 and an increase in A. In addition, since μ increases, b must decrease. Since there is a change in μ it is necessary to use a different *RAPAD* before and after modification.

f. Updraft (Fig. 10.3f)

Because of the retarding influence of gravity preferably on the larger drops, an updraft eliminates the smallest precipitation particles from the RDSD at the lower levels. This is especially true in thunderstorms, where the smallest particles are deposited in the anvil or are carried aloft to other regions where they fall out later. The effect on the RDSD is therefore the same as evaporation.

g. Downdraft (Fig. 10.3g)

A downdraft would increase the downward flux of particles of all diameters. A change in the shape of the RDSD is likely, but the details of the changes are not certain. One possible modification is shown in Fig. 10.3g. Should such changes in RDSD shape occur it would necessitate the use of a different RAPAD before and after modification.

h. Size sorting (Fig. 10.3h)

Size sorting tends to make the RDSD much narrower, which means μ must increase substantially. Therefore, b must decrease. Obviously N_T must decrease, but what happens to D_0 depends on which segment of the precipitation streamer is being observed. So A would either increase or decrease depending on what happens to D_0. It is likely that the decrease in N_T will dominate the change in D_0 so that A would increase, but this is not certain. Because of the dramatic change in μ a different RAPAD would have to be used before and after modification.

4. Conceptual model of rain formation

In the present work a review is presented of the physical considerations enumerated above and a test is made against the wealth of RDSD-based Z–R relations that have been reported during the last five decades. Our departure point is the equilibrium drop-size distribution (DSDe). In that regard the theoretical calculations of the DSDe of Hu and Srivastava (1995) are used in this work. We applied the method of moments [as described by Tokay and Short (1996)] to the DSDe data of Hu and Srivastava (1995) and found values of $\mu = 9$, $D_0 = 1.76$ mm, and a Z–R relation of the form $Z = 600\ R$. A RAPAD corresponding to this value of μ is shown in Fig. 10.4, in which a point corresponding to the DSDe is shown as the large filled circle. Also shown are the four Z–R relations depicted by Atlas and Chmela (1957) on their RAPAD. It is notable that, when extended to

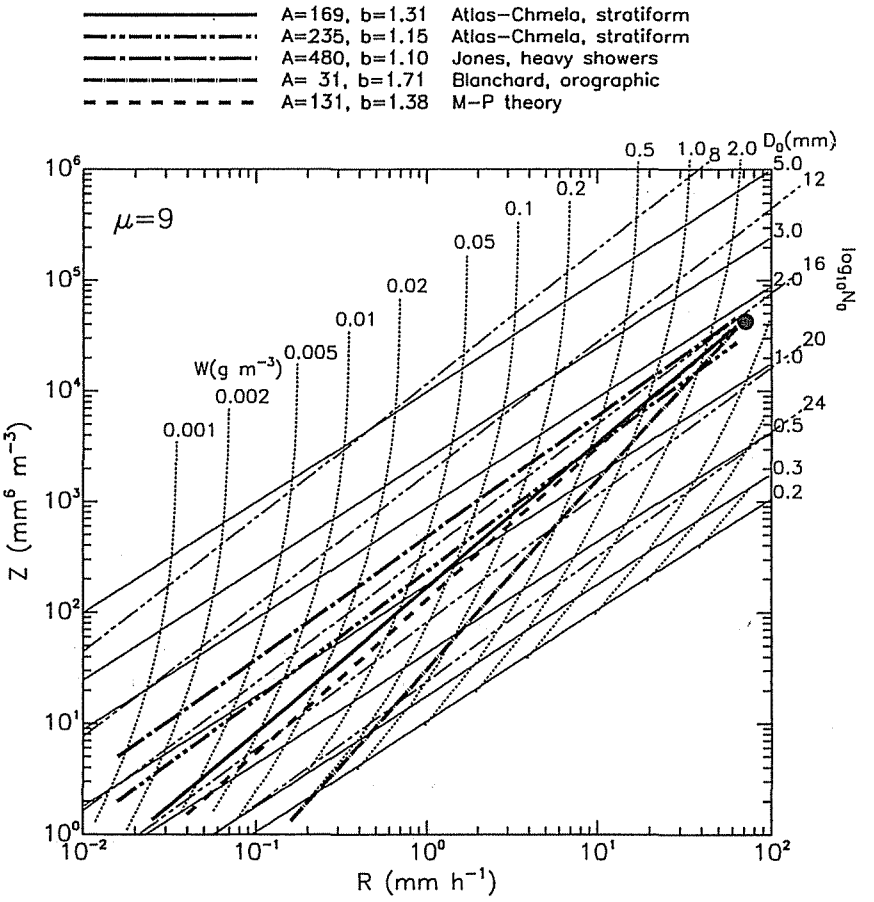

FIG. 10.4. Rain parameter diagram for a gamma distribution with $\mu = 9$. Isopleths are the same as in Fig. 10.1. Also shown are the four Z–R relations displayed by Atlas and Chmela (1957). The large filled circle corresponds to the theoretical equilibrium RDSD of Hu and Srivastava (1995) for which $\mu = 9$ and $D_0 = 1.76$ mm. It is notable that the four Z–R relations are close to converging to the point for the equilibrium distribution.

large rainfall rates, these four relations tend to converge to the DSDe.

a. Equilibrium DSD and Z–R relations

The DSDe is the drop-size distribution that would be developed in a rain shaft that falls a sufficiently long time for the rates of drop merging and breakup processes to reach equilibrium, assuming no gain or loss of raindrops to other processes. The time required for reaching DSDe is shorter for greater R, because of the greater W and respectively shorter time between drop interactions. Hu and Srivastava (1995) have calculated that reaching DSDe from initial Marshall–Palmer exponential RDSD would take about 10 min for $R = 90$ mm h^{-1}, but the main features of DSDe would appear already after 2.5 min. The time for reaching DSDe becomes longer linearly with R^{-1}. Hu and Srivastava (1995, p. 1768) stated that "for heavy rainfall rates, say 50 mm h^{-1}, approximate equilibrium between collisional processes may perhaps be expected within the usual lifetime of a convective shower." Supporting observations in heavy tropical rain showers were reported by Zawadzki and de Agostinho Antonio (1988). Observations at extratropical rain showers showed considerable deviations from DSDe (Carbone and Nelson 1978; Sauvageot and Lacaux 1995).

Because DSDe is independent of R, D_0 is constant at 1.76 mm, and R is linear with N_T. This means that the exponent in the Z–R power-law relation is unity (List 1988), and the Z–R relation is simply $Z = 600\,R$ (after Hu and Srivastava 1995). An exponent greater than 1 means that D_0 is increasing with R. During the growth phase of the precipitation before reaching DSDe, D_0 does increase with R. The conversion of cloud droplets to precipitation occurs by forming small precipitation particles that increase in size with the progress of their collection of the cloud water and so increasing R, until the drops become sufficiently large for breakup to compensate their additional growth. Because breakup does not occur in convective ice precipitation, that is, graupel and hail, no equilibrium is expected there and the equiv-

alent melted hydrometeors would have ever-increasing D_0 with R. This is why rain formed from the melting of hail can reach extreme reflectivities, which translate to impossibly high R when applying to the hail Z–R relations for rainfall.

b. Evolution of warm rain

In a hypothetical rising cloud column with active coalescence, the initial dominant process would be widening of the cloud drop-size distribution into large concentrations of drizzle drops; the drizzle continues to coalesce with other drizzle and cloud drops into raindrops, which will continue to grow asymptotically to D_{0e}. Therefore, during the growth phase of precipitation R increases with D_0, and this would increase the exponent b. Ideally, for rainfall with drops that fall from cloud top while growing, R would increase with the fall distance from the cloud top, mainly by growth of the falling drops due to accretion and coalescence, and to a lesser extent by addition of new small rain drops, until R becomes sufficiently large for breakup to become significant. Shallow orographic clouds can present conditions such as some distance below the tops of convective clouds. Therefore, similar evolution of R can be observed on a mountain slope, such as documented by Fujiwara (1965). Different values of R near cloud top or in shallow orographic clouds can come mainly from changing N_T, because the drop size is bounded by the limited vertical fall distance along which they can grow. This would cause orographic precipitation to have small coefficient A, and more so with shallower clouds and stronger orographic ascent, because the stronger rising component supplies more water for the production of many small raindrops not too far below cloud top, which are manifested as a larger R.

c. Evolution of cold rain

Microphysically "continental" clouds are characterized by narrow cloud drop-size distributions and, therefore, by having little drop coalescence and warm rain. Most raindrops originate from melting of ice hydrometeors that are typically graupel or hail in the convective elements, and snowflakes in the mature or stratiform clouds. Graupel and hail particles grow without breakup while falling through the supercooled portion of the cloud, and continue to grow by accretion in the warm part of the cloud, where they melt. Large melting hailstones shed the excess meltwater in the form of an RDSD about which little is known. The shedding stops when the melting particles approach the size of the largest stable raindrops, which are later subject to further breakup due to collisions with other raindrops. In fact, new raindrop formation is limited only to the breakup of pre-existing larger precipitation particles. Therefore, we should expect that in such clouds there would be, for a given R, a relative dearth of small drops and excess of large drops compared to microphysically "maritime" clouds with active cloud drop coalescence. Deep continental convective clouds would therefore initiate the precipitation by forming large drops that, with maturing, approach DSDe from above. This is in contrast with the approach from below for maturing maritime RDSD.

Recent satellite studies (Rosenfeld and Lensky 1998) have shown that microphysically maritime clouds are associated typically with a "rain-out" zone; that is, the fast conversion of cloud water to precipitation causes the convective elements to lose water to precipitation while growing. This leaves less water carried upward to the supercooled zone, so that weaker ice precipitation can develop aloft. Williams et al. (2002) have recognized this as a potential cause to the much greater occurrence of lightning in continental compared to maritime clouds. Williams et al. (2002) noted that frequent lightning occurred also in very clean air during high atmospheric instability, probably because the strong updraft leaves little time to the formation of warm rain and carries the large raindrops that manage to form up to the supercooled levels of the clouds, where they freeze and participate in the cloud electrification processes.

This difference between continental and maritime clouds means that mostly warm rain would fall even from the very deep maritime convection, which reaches well above the freezing level, whereas precipitation from continental clouds would originate mainly in ice processes. Therefore, the expected difference in RDSD between microphysically maritime and continental clouds is expected to exist also for the deepest convective clouds that extend well into the subfreezing temperatures.

5. Proposed method of classifying Z–R relations

Equipped with this conceptual model, now we can turn our attention to actual measurements of RDSDs and their Z–R relations, which can be related to the precipitation-forming processes as discussed above. These Z–R relations are provided in Table 10.5 and are classified according to combinations of the categories of microphysically maritime and continental, convective, stratiform, and orographic. The values of A and b are those listed in the source of the Z–R relation, whereas the values of the RDSD parameters N_0 and μ were calculated from A and b using Eqs. (10.23) and (10.24), respectively. The coefficients and exponents (ε, δ) and (ζ, κ) in the D_0–R and W–R relations, respectively, were calculated using the expressions in Table 10.3. Also shown for reference in Table 10.5 are values of $D_0(10)$, $D_0(30)$, $W(10)$, and $W(30)$, the values of D_0 and W at $R = 10$ and 30 mm h^{-1}. It should be recognized that the D_0–R and W–R relations derived in this way are strictly theoretical and are only approximations to those that might be found from empirical analyses of the data from which the Z–R relations were found. However, in

TABLE 10.5. RDSD parameters μ and N_0 deduced from values of A and b in $Z = AR^b$ for the sources shown in the second column. Also shown are the theoretical values of the coefficients and exponents (ε, δ), and (ζ, κ) in the corresponding D_0–R and W–R relations of the form $Y = cX^d$, where D_0 is the median volume diameter (cm) and W is the liquid water concentration (g m^{-3}). The reference number in the first column refers to the description of the data given in part (b) of the table. Values of D_0 and W for R = 10 and 30 mm h^{-1} are listed in the columns labelled $D_0(10)$, $D_0(30)$, $W(10)$, and $W(30)$, respectively.

Ref.	Source	A	b	μ	N_0	ε	δ	ζ	κ	$D_0(10)$	$D_0(30)$	$W(10)$	$W(30)$
a) Parameters													
1	Joss and Waldvogel (1970)	830	1.50	−0.010	0.634D+04	0.148	0.215	0.055	0.856	0.243	0.308	0.393	1.007
2	Foote (1966)	646	1.46	0.395	0.321D+05	0.137	0.197	0.058	0.868	0.216	0.269	0.426	1.106
3	Rinehart (2002)	429	1.59	−0.721	0.289D+04	0.104	0.215	0.069	0.830	0.187	0.246	0.466	1.160
4	Sims (1964)	446	1.43	0.749	0.201D+06	0.120	0.185	0.063	0.876	0.183	0.225	0.478	1.251
5	Petrocchi and Banis (1980)	316	1.36	1.802	0.112D+08	0.109	0.155	0.068	0.896	0.156	0.184	0.536	1.435
6	Sauvageot (1994)	425	1.29	3.364	0.458D+09	0.130	0.124	0.061	0.917	0.174	0.199	0.500	1.369
7	Ulbrich et al. (1999)	261	1.43	0.749	0.700D+06	0.095	0.185	0.074	0.876	0.146	0.178	0.557	1.459
8	Maki et al. (2001)	232	1.38	1.462	0.892D+07	0.094	0.163	0.075	0.891	0.137	0.164	0.583	1.551
9	Tokay et al. (1995)	175	1.37	1.627	0.324D+08	0.084	0.159	0.081	0.894	0.121	0.144	0.634	1.691
10	Tokay and Short (1996)	139	1.43	0.749	0.303D+07	0.073	0.185	0.089	0.876	0.111	0.136	0.668	1.749
11	Stout and Mueller (1968)	126	1.47	0.287	0.772D+06	0.068	0.202	0.093	0.865	0.108	0.134	0.681	1.761
12	Stout and Mueller (1968)	146	1.42	0.878	0.418D+07	0.075	0.180	0.087	0.879	0.113	0.138	0.660	1.734
13	Tokay et al. (1995)	335	1.37	1.627	0.560D+07	0.111	0.159	0.067	0.894	0.160	0.190	0.526	1.403
14	Tokay and Short (1996)	367	1.30	3.097	0.344D+09	0.122	0.129	0.063	0.914	0.163	0.188	0.520	1.420
15	Stout and Mueller (1968)	226	1.46	0.395	0.315D+06	0.088	0.197	0.078	0.868	0.138	0.171	0.577	1.496
16	Ulbrich and Atlas (2001)	120	1.43	0.749	0.426D+07	0.068	0.185	0.093	0.876	0.104	0.128	0.697	1.824
17	Ulbrich and Atlas (2001)	203	1.46	0.395	0.398D+06	0.084	0.197	0.081	0.868	0.132	0.164	0.595	1.543
18	Jorgensen and Willis (1982)	287	1.27	3.960	0.110D+11	0.112	0.116	0.067	0.922	0.146	0.166	0.562	1.549
19	Jorgensen and Willis (1982)	301	1.38	1.462	0.450D+07	0.105	0.163	0.070	0.891	0.153	0.183	0.541	1.439
20	Fujiwara and Yanase (1968)	240	1.48	0.184	0.141D+06	0.088	0.206	0.078	0.862	0.142	0.178	0.564	1.455
21	Fujiwara and Yanase (1968)	88	1.28	3.651	0.291D+12	0.067	0.120	0.095	0.919	0.088	0.101	0.788	2.164
22	Fujiwara and Yanase (1968)	48	1.11	16.512	0.436D+34	0.058	0.047	0.105	0.968	0.065	0.068	0.976	2.828
23	Blanchard (1953)	31	1.71	−1.388	0.159D+05	0.031	0.305	0.155	0.796	0.062	0.086	0.967	2.318

TABLE 10.5. (*Continued*)

(b) Source and notes.	
Continental	
1. Joss and Waldvogel (1970)	Thunderstorms. 25 days total, Locarno, Switzerland. Disdrometer data.
2. Foote (1966)	Mountain thunderstorm in AZ. Filter paper measurements. 62 spectra for 37 storms.
3. Rinehart (2002)	Grand Forks, ND during several autumn seasons. Filter paper measurements.
4. Sims (1964)	Thundershowers, 1963. ISWS drop camera data.
Moderate continental	
5. Petrocchi and Banis (1980)	Thunderstorm, Norman, OK. Disdrometer data.
Tropical continental	
6. Sauvageot (1994)	Tropical squall line. Congo. Disdrometer data.
7. Ulbrich et al. (1999)	Average of seven afternoon thunderstorms in Arecibo, PR. Disdrometer data.
8. Maki et al. (2001)	Darwin, Australia, 1997–98. 15 squall lines, all stages. Disdrometer data.
Tropical maritime	
9. Tokay et al. (1995)	Tropical maritime, coastal, convective, Darwin, Australia. Disdrometer data.
10. Tokay and Short (1996)	Tropical convective, equatorial, maritime, TOGA COARE, Disdrometer data.
11. Stout and Mueller (1968)	Marshall Islands, trade wind cumulus, warm rain, maritime. ISWS drop camera data.
12. Stout and Mueller (1968)	Marshall Islands, showers, equatorial maritime. ISWS drop camera data.
13. Tokay et al. (1995)	Darwin, Australia. Stratiform, coastal, tropical maritime. Disdrometer data.
14. Tokay and Short (1996)	TOGA COARE, stratiform, coastal, equatorial maritime. Disdrometer data.
15. Stout and Mueller (1968)	Marshall Islands, continuous rain. Equatorial maritime. ISWS drp camera data.
Tropical maritime aloft	
16. Ulbrich and Atlas (2001)	TOGA COARE Convective aloft, by updraft. PMM analysis. 2DP probe data.
17. Ulbrich and Atlas (2001)	TOGA COARE Stratiform aloft, by updraft. PMM analysis. 2DP probe data.
Hurricane	
18. Jorgensen and Willis (1982)	Hurricane eye wall. Aircraft data aloft. 2DP probe data.
19. Jorgensen and Willis (1982)	Hurricane rain bands. Aircraft data aloft. 2DP probe data.
Orographic	
20. Fujiwara and Yanese (1968)	Orographic rain, Mount Fuji at altitude of 1300 m. Filter paper.
21. Fujiwara and Yanese (1968)	Orographic rain, Mount Fuji at altitude of 2100 m. Filter paper.
22. Fujiwara and Yanese (1968)	Orographic rain, Mount Fuji at altitude of 3400 m. Filter paper.
23. Blanchard (1953)	Orographic rain, Hawaii, Mauna Loa, altitudes between 670–920 m. Filter paper.

the vast majority of the empirical Z–R relations investigated in this work there is no information available concerning the corresponding D_0–R and W–R relations. The method employed in this work finds theoretical D_0–R and W–R relations that are used for classifying the type of rainfall even though they may not be accurate representations of the actual empirical relations. Nevertheless, Atlas (1964) has shown that the D_0–R relations found from the Z–R relations he investigated are in good agreement with those found directly from empirical analysis of experimental drop-size spectra. In Figs. 10.6, 10.9, 10.11, and 10.12 that follow, theoretical D_0–W relations are plotted for values of $\mu = -2$ and 12 and for $R = 10$ and 30 mm h^{-1}. These relations are found from Eq. (10.15) using the definitions in Table 10.3 and have the form

$$\frac{W}{R} = 0.0157(3.67 + \mu)^{0.67}\frac{\Gamma(4 + \mu)}{\Gamma(4.67 + \mu)}D_0^{-0.67}. \quad (10.26)$$

The two curves in each figure represent the range of uncertainty (for given R) in nature associated with the theoretical relations. In all cases it is seen that the the uncertainty due to such variations is small, thus adding further credibility to the method of classifying the Z–R relations.

a. Maritime–continental classification

The most fundamental classification of rain clouds can be done into maritime and continental. Cloud physicists have traditionally designated clouds as maritime and continental based on their microstructure, where maritime clouds contain small concentrations (about 50–100 cm^{-3}) of large droplets, and continental clouds contain tenfold-larger concentrations of respectively smaller droplets. Maritime clouds precipitate easily by warm processes, whereas coalescence is often suppressed in continental clouds, which often have to grow to supercooled levels to precipitate by "cold" processes, that is, involving the ice phase. Some notable differences have been documented between maritime and continental convective clouds.

- There is distinctly less supercooled water and it is limited to warmer temperatures in the tropical maritime compared to the continental clouds (Zipser and LeMone 1980; Black and Hallett 1986).
- The updraft velocities in maritime clouds are characteristically limited to below the terminal fall velocity of the raindrops, whereas no such maximum for the updraft was noted in continental convection (Zip-

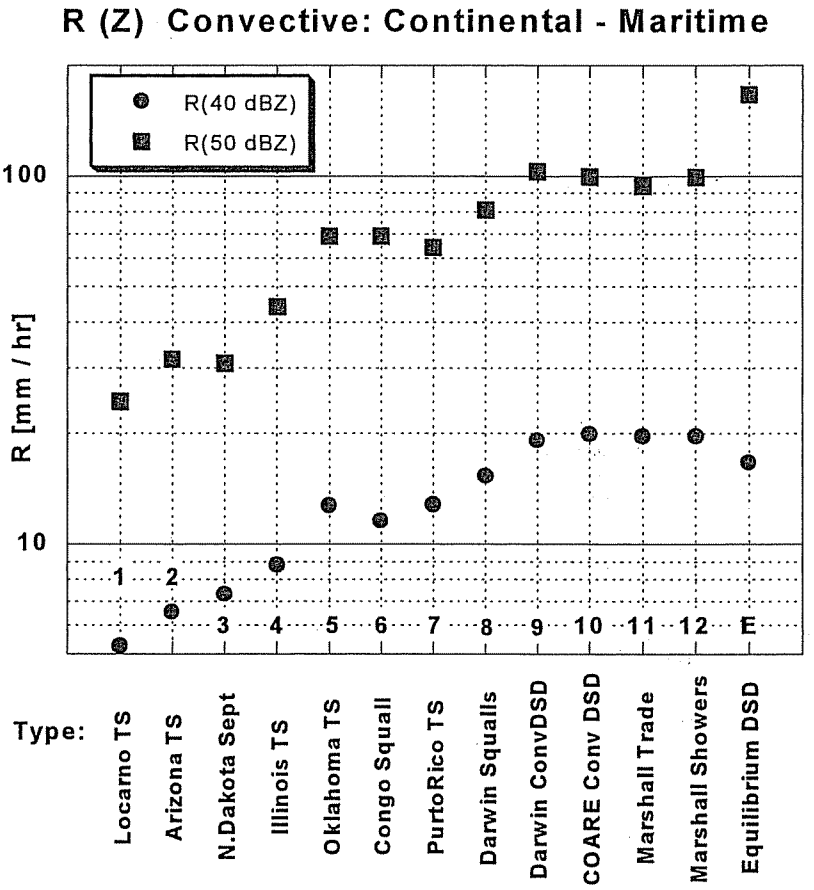

FIG. 10.5. The Z–R relations for rainfall from maritime and continental convective clouds. The rain intensities for 40 and 50 dBZ are plotted in the figure. Note the systematic increase of R for a given Z for the transition from continental to maritime clouds. The Z–R relations used in this figure are as follows:

	A	b
1. Swiss Locarno thunderstorms, continental (Joss and Waldvogel 1970)	830	1.50
2. Arizona mountain thunderstorms (Foote 1966)	646	1.46
3. Grand Forks, North Dakota, in autumn (R. E. Rinehart 2002, personal communication)	429	1.59
4. Illinois thunderstorms, continental (Sims 1964)	446	1.43
5. Oklahoma thunderstorms, moderate continental (Petrocchi and Banis 1980)	316	1.36
6. Congo squall line, tropical continental (Sauvageot 1994)	425	1.29
7. Puerto Rico thunderstorms, coastal, moderate maritime (Ulbrich et al. 1999)	261	1.43
8. Darwin Squalls, coastal, tropical maritime (Maki et al. 2001)	232	1.38
9. Darwin convective DSD, coastal, tropical maritime (Tokay et al. 1995)	175	1.37
10. COARE convective DSD, equatorial maritime (Tokay and Short 1996)	139	1.43
11. Marshall trade wind cumulus, warm rain maritime (Stout and Mueller 1968)	126	1.47
12. Marshall Showers, equatorial maritime (Stout and Mueller 1968)	146	1.42
E. Equilibrium DSD	600	1.00

ser and LeMone 1980; Jorgensen and LeMone 1989; Zipser and Lutz 1994).

- The vertical profiles of radar reflectivity in the mixed-phase region are substantially stronger in continental than in maritime clouds. This was ascribed mainly to the greater updraft velocities in the more continental conditions (Williams et al. 1992; Rutledge et al. 1992; Zipser 1994; Zipser and Lutz 1994).
- All of these differences can potentially explain the dramatic contrast between the lightning over land and ocean that was revealed when observations of lightning from space became available (Orville and Henderson 1986).

Given the fundamental importance of the classification of clouds into maritime and continental, and in view of

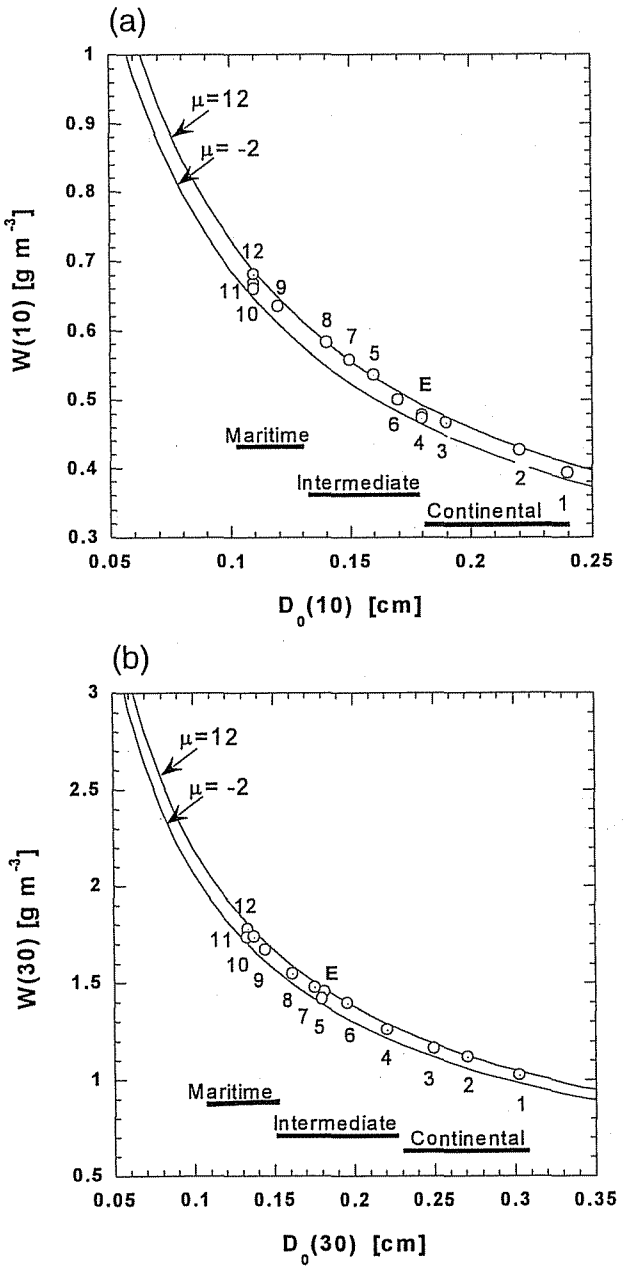

FIG. 10.6. (a) The liquid water content W vs median volume diameter D_0 for $R = 10$ mm h^{-1} of convective rainfall in maritime and continental regimes. The label of the points is according to Fig. 10.5. Note that D_0 decreases for more maritime clouds. The curves labeled with values of μ are theoretical D_0–W relations for $R = 10$ mm h^{-1}. The range of values of μ from -2 to 12 represent the range of observed variability of the D_0–W relations that would be expected in nature. Curves for values of μ greater than 12 are identical to that for $\mu = 12$. (b) The liquid water content W vs median volume diameter D_0 for $R = 30$ mm h^{-1} of convective rainfall in maritime and continental regimes. The label of the points is according to Fig. 10.5. Note that D_0 decreases for more maritime clouds. Also note that D_0 for maritime clouds is smaller than the equilibrium D_{0e} and vice versa for rainfall from continental clouds. Other details are the same as in (a).

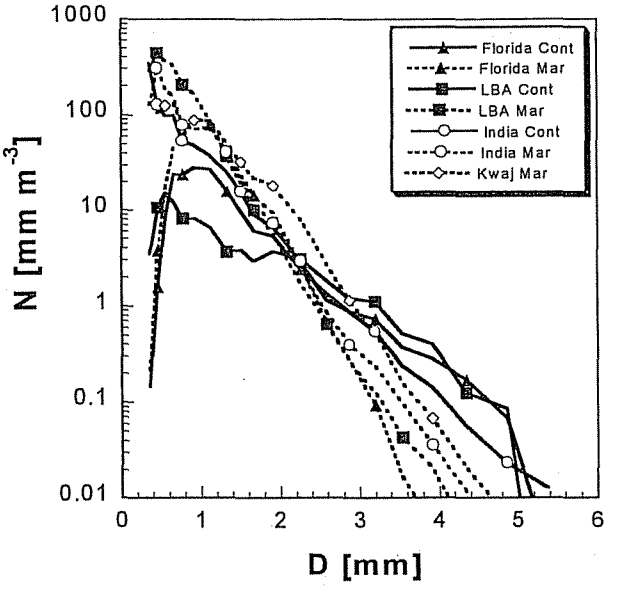

FIG. 10.7. Disdrometer-measured RDSDs of continental and maritime rainfall, as micophysically classified by VIRS overpass. The RDSD is averaged for the rainfall during ±18 h of the overpass time, and the concentrations are scaled to 1 mm h^{-1}. The disdrometers are in Florida (Teflun B), Amazon (LBA), India (Madras), and Kwajalein.

the implications to RDSD as alluded to in the section describing the conceptual model, it is expected that systematic differences in RDSD would also be ordered by this classification. The classification was done on all of the Z–R relations available to us that were based on RDSD measurements and could be related to a relative scale of estimated continentality–maritimity of the clouds. Figure 10.5 presents 12 such Z–Rs, ordered from extreme continental through moderate continental, tropical continental, moderate maritime, to equatorial maritime. According to Fig. 10.5, R increases for a given Z with increasing maritimity of the clouds, by a factor of more than 3. This substantial factor is the manifestation of major differences in the RDSD for continental and maritime clouds. Figures 10.6a,b illustrate the dependence of the drop sizes and number concentrations on the continentality of the clouds, based on the RDSD parameters that are calculated in Table 10.5. According to Fig. 10.6, D_0 increases systematically from maritime to continental clouds, reaching the greatest value in the most extreme continental clouds in Switzerland and in Arizona. At $R = 30$ mm h^{-1} (Fig. 10.6b) the drops are larger than the equilibrium DSD ($D_0 > D_{0e}$) for continental clouds, and $D_0 < D_{0e}$ for maritime clouds, in agreement with the conceptual model. This explains the substantial decrease of R for the same Z in more continental clouds, as shown in Fig. 10.5.

Is it the microstructure of the cloud or the impact of the surface properties (land or ocean) that makes the clouds continental or maritime and so produces such vastly different RDSDs? There is no clear separation between these two alternatives, because both aerosol

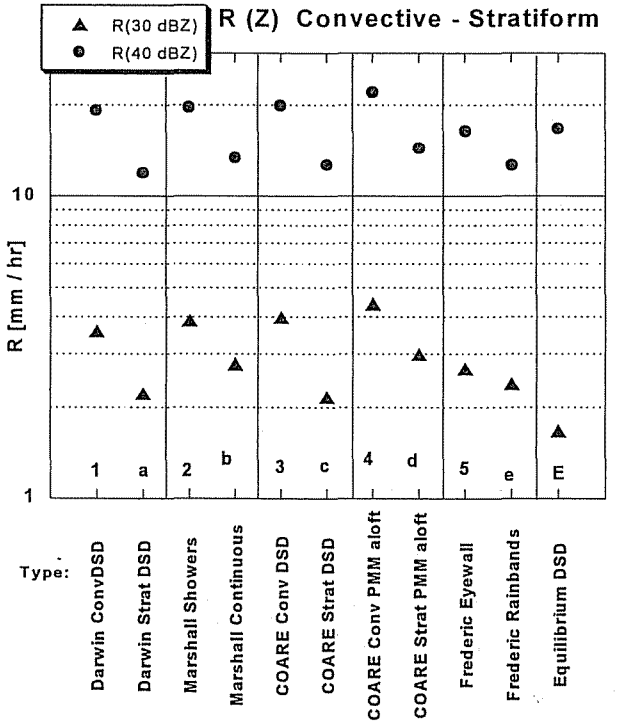

FIG. 10.8. The Z–R relations for rainfall from convective and stratiform tropical rainfall and from a hurricane. The rain intensities for 30 and 40 dBZ are plotted in the figure. Note the systematic increase of R for a given Z for the transition from stratiform to convective clouds. Apparently hurricane rainfall is more similar to stratiform, even in the eyewall. The Z–R relations used in this figure, numbered in digits for convective and characters for stratiform, are as follows:

		A	b
1.	Darwin convective DSD, coastal, tropical maritime (Tokay et al. 1995)	175	1.37
a.	Darwin stratiform DSD, coastal, tropical maritime (Tokay et al. 1995)	335	1.37
2.	Marshall showers, equatorial maritime (Stout and Mueller 1968)	146	1.42
b.	Marshall continuous, equatorial maritime (Stout and Mueller 1968)	226	1.46
3.	COARE convective DSD, equatorial maritime (Tokay and Short 1996)	139	1.43
c.	COARE stratiform DSD, equatorial maritime (Tokay and Short 1996)	367	1.30
4.	COARE convective aloft, by updraft (Ulbrich and Atlas 2002)	120	1.43
d.	COARE stratiform aloft, by updraft (Ulbrich and Atlas 2002)	203	1.46
5.	Hurricane eyewall (Jorgensen and Willis 1982)	287	1.27
e.	Hurricane rainbands (Jorgensen and Willis 1982)	301	1.38
E.	Equilibrium DSD	600	1.00

content and updraft velocities determine cloud microstructure. Larger aerosol concentrations make the coalescence slower, and greater updrafts leave less time for the progress of the coalescence, so that the product of these two factors ultimately determines the "continentality" of the clouds, as manifested by the evolution of cloud drop-size distribution with height in the growing convective elements. The ultimate test for the role of cloud microstructure is comparing the RDSD of clouds at the same location, but at different times, when they possess maritime or continental microstructure.

That is exactly what is done in Fig. 10.7. The visible and infrared scanner onboard (VIRs) the Tropical Rainfall Measuring Mission (TRMM) satellite was used to retrieve the microstructure of rain clouds over disdrometer sites. The clouds were classified into continental, intermediate, and maritime, using the methodology of Rosenfeld and Lensky (1998). The DSDs from the continental and maritime classes during the overpass time ± 18 h were lumped together and plotted in Fig. 10.7. Indeed, the continental and maritime DSDs are well separated in Fig. 10.7, with the continental clouds producing greater concentrations of large drops and smaller concentrations of small drops. A comparison between the directly measured disdrometer rainfall and the calculated accumulation by applying the TRMM Z–R relations (Iguchi et al. 2000) to the disdrometer measured Z resulted in a relative overestimate by more than a factor of 2 of the rainfall from the microphysically continental clouds compared to the maritime clouds.

The evidence shows that it is mainly the cloud microstructure that is responsible to the large systematic difference in the RDSD and Z–R relations between maritime and continental clouds. There are several possible causes for these differences, as described in the following sections, all working at the same direction.

1) EXTENT OF COALESCENCE

The cloud drop coalescence in highly maritime clouds is so fast that rainfall is developed low in the growing convective elements and precipitates while the clouds are still growing. The large concentrations of raindrops that form low in the cloud typically fall before they have the time to grow and reach equilibrium RDSD, thereby creating the rain-out zone (Rosenfeld and Lensky 1998) less than 2 km above cloud-base height. Therefore, D_0 remains much smaller than D_{0e}, as can be seen in Fig. 10.6b.

In microphysically continental clouds with suppressed coalescence the cloud has to grow into large depth before it will start precipitating, by either warm or cold processes. The raindrops that fall through the lower part of the cloud grow by accretion of small cloud drops, so that they tend to break up much less than drops that grow mainly by collisions with other raindrops, as is the case for maritime clouds. This process allows D_0 to exceed D_{0e} in the growing stages of the precipitation and later to approach it from above when the raindrop collisions become more frequent with the intensification of the rainfall.

2) WARM VERSUS COLD PRECIPITATION PROCESSES

The rain-out of the maritime clouds (Rosenfeld and Lensky 1988) depletes the cloud water before reaching

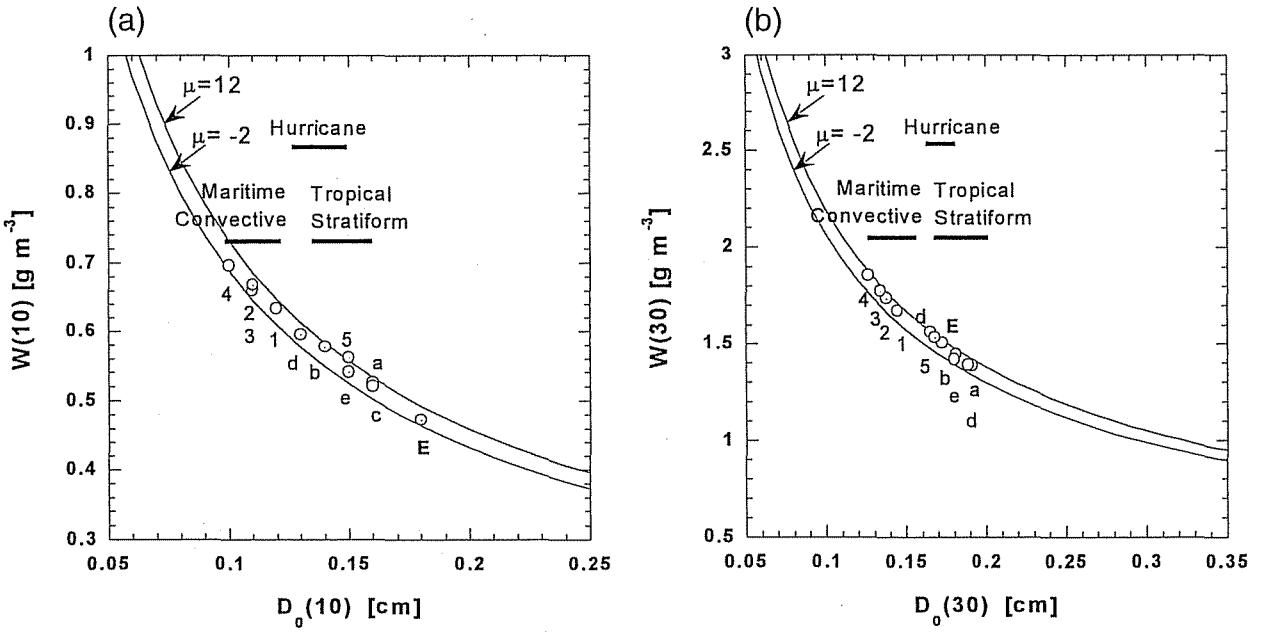

FIG. 10.9. (a) The liquid water content W vs median volume diameter D_0 for R = 10 mm h^{-1} from convective and stratiform tropical rainfall, and from a hurricane. The labels of the points are according to Fig. 10.8. Other details are the same as in Fig. 10.6a. (b) The liquid water content W vs median volume diameter D_0 for R = 30 mm h^{-1} from convective and stratiform tropical rainfall and from a hurricane. The labels of the points are according to Fig. 10.8. Note the distinct separation into convective and stratiform groups, where the convective rainfall has much smaller D_0. The hurricane rainfall fits into the stratiform group. Other details are the same as in Fig. 10.6a.

the supercooled levels (Zipser and LeMone 1980; Black and Hallett 1986), so that mixed-phase precipitation would be much less developed in the maritime clouds compared to the continental. This is manifested in the smaller reflectivity aloft in the maritime clouds (Zipser and Lutz 1994), which is a manifestation of the smaller hydrometeors that form there (Zipser 1994). In contrast, the suppressed coalescence in continental clouds leaves most of the cloud water available for growth of ice hydrometeors aloft, typically in the form of graupel and hail. These ice hydrometeors can grow indefinitely without breakup, until they fall into the warm part of the cloud and melt. The melted hydrometeors continue to grow by accretion of cloud droplets, until they exceed the size of spontaneous breakup or collide with other raindrops. Therefore, convective rainfall that originates as ice hydrometeors would have $D_0 > D_{0e}$ and would approach D_{0e} from above with maturing of the RDSD.

3) STRENGTH OF THE UPDRAFTS

Updrafts are typically stronger in more continental clouds and therefore contribute to more microphysically continental clouds and less warm rain processes, as discussed already above. In addition, stronger updrafts allow drops with greater minimal size to fall through them. In addition, stronger updrafts leave less time for forming of warm rain and rain-out, and advect more cloud water to the supercooled zone. Therefore, due to the reasons already discussed in sections 5a(1) and 5a(2), the stronger updrafts are likely to lead to precipitation with greater D_0 and smaller R for the same Z.

4) EVAPORATION

More continental environments have typically higher cloud base and lower relative humidity at the subcloud layer. Evaporation depletes preferentially the smaller raindrops and works to increase D_0.

b. Convective–stratiform classification

The mature elements of organized deep convective cloud systems often merge into widespread light to moderate rainfall area, which is called "stratiform," although it is eventually generated by convection. The classification is obvious in typical squall lines, which have a simple structure with three characteristic regions: convective, stratiform, and transition (Houze 1989). The rainfall in the convective and transition regions is formed as warm rain and graupel melt. Typically, there is more warm rain falling through the updraft, and more graupel melt falling with the downdraft toward the transition zone. The stratiform precipitation is composed typically of ice particles that were advected from the convective portion of the storm, and from aggregation of newly formed ice crystals in the moderate mesoscale updraft that develops in the merged anvils over the stratiform rainfall area. Waldvogel (1974) has shown that the onset of the stratiform precipitation is associated

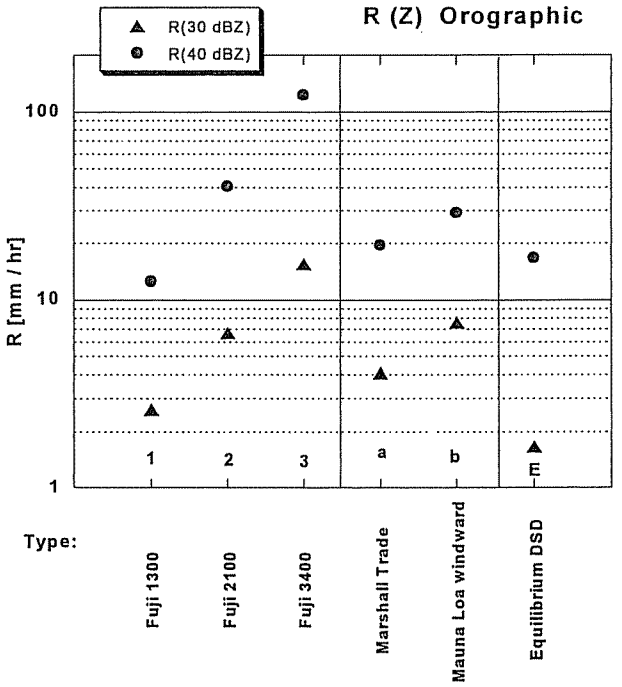

FIG. 10.10. The Z–R relations for warm rain over orographic barriers. The rain intensities for 30 and 40 dBZ are plotted in the figure. Note the systematic increase of R for a given Z for a greater height of the sampling location. The Z–R relations used in this figure, numbered in digits for Mount Fuji and characters for Hawaii, are as follows:

	A	b
1. Mount Fuji, at height of 1300 m (Fujiwara and Yanase 1968)	240	1.48
2. Mount Fuji, at height of 2100 m (Fujiwara and Yanase 1968)	88	1.28
3. Mount Fuji, at height of 3400 m (Fujiwara and Yanase 1968)	48	1.11
a. Marshall trade wind cumulus, warm rain maritime (Stout and Mueller 1968)	126	1.47
b. Hawaii, windward side of Mauna Loa, at 670–920 m (Blanchard 1953)	31	1.71
E. Equilibrium DSD	600	1.00

with sharp decrease of N_0, leading to greater Z for the same R. This was ascribed to the aggregation of the ice particles (Stewart et al. 1984), as evident by the bright band that is typically associated with the stratiform rainfall with large drops (Huggel et al. 1996). Substantial fraction of the stratiform rainfall can evaporate during its long fall from the melting level, so that the smaller drops evaporate preferentially, with further decrease in N_0 and increase in D_0.

The differences between convective and stratiform DSD are probably the best recognized and documented, mainly in the context of tropical rainfall. The DSD-based Z–Rs available to us were compiled in Fig. 10.8. According to the figure, the same Z translates to R greater by a factor of 1.5–2 in maritime convective compared to stratiform rainfall.

The convective and stratiform rainfall is nicely separated in Fig. 10.9 by the values of D_0, where, as expected, D_0 is much greater for stratiform than convective rainfall. Stratiform rainfall usually occurs at $R < 15$ mm h^{-1}. The extrapolation of stratiform rain to 30 mm h^{-1} in Fig. 10.9b is rarely achieved, except for in hurricanes. The eyewall and rainbands in hurricanes are not considered normally as stratiform because R often exceeds 15 mm h^{-1}. However, according to Figs. 10.8 and 10.9, at least the Z–R and D_0 of hurricane Frederic had stratiform values. The eyewall value of D_0 was somewhat smaller and thus more convective than D_0 of the rainbands, but still closer to the stratiform than the convective range of values.

As expected for such a mature and deep rain system, the values of D_0 in the hurricane are not far from D_{0e}, especially for the larger rain intensities. For regular stratiform rain, D_0 is still much smaller than D_{0e}, suggesting that the raindrop coalescence and breakup do not play a major role in shaping the stratiform RDSD.

c. *Orographic rainfall classification*

The few available RDSDs for orographic rain are compiled in Figs. 10.10 and 10.11. According to the figures, orographic lifting of maritime air can supply a large amount of condensates, which create a large numer of small raindrops that fall to the mountain slope. This highly immature RDSD has extremely small D_0, which leads to very small Z for a given R. According to Fig. 10.10, the low-level (i.e., close to the ground) orographic enhancement can cause an underestimate of R by up to a factor of 10, when using the same Z–R as for the upwind rainfall. This low-level enhancement depends on effective cloud drop coalescence. Therefore, the low-level enhancement probably would be weaker in more microphysically continental clouds, with respectively less radar underestimate of its magnitude.

6. Summary

The longstanding question of RDSD and Z–R relationships has been revisited in this work, this time from the combined approach of rain-forming physical processes that shape the RDSD, and a formulation of the RDSD into the simplest free parameters of R, W, and D_0. It was found that the major processes that shape RDSD are, by order of practical importance as viewed by the authors,

a) cloud microstructure, with the two end members being (i) microphysically continental with small cloud drops, suppressed cloud drop coalescence and warm rain processes and with strong updrafts; and (ii) microphysically maritime with large cloud drops, active coalescence and warm rain, and weak updrafts;
b) cloud dynamics, with the two end members being (i) "convective," where precipitation elements grow in convective updrafts by coalescence and accretion

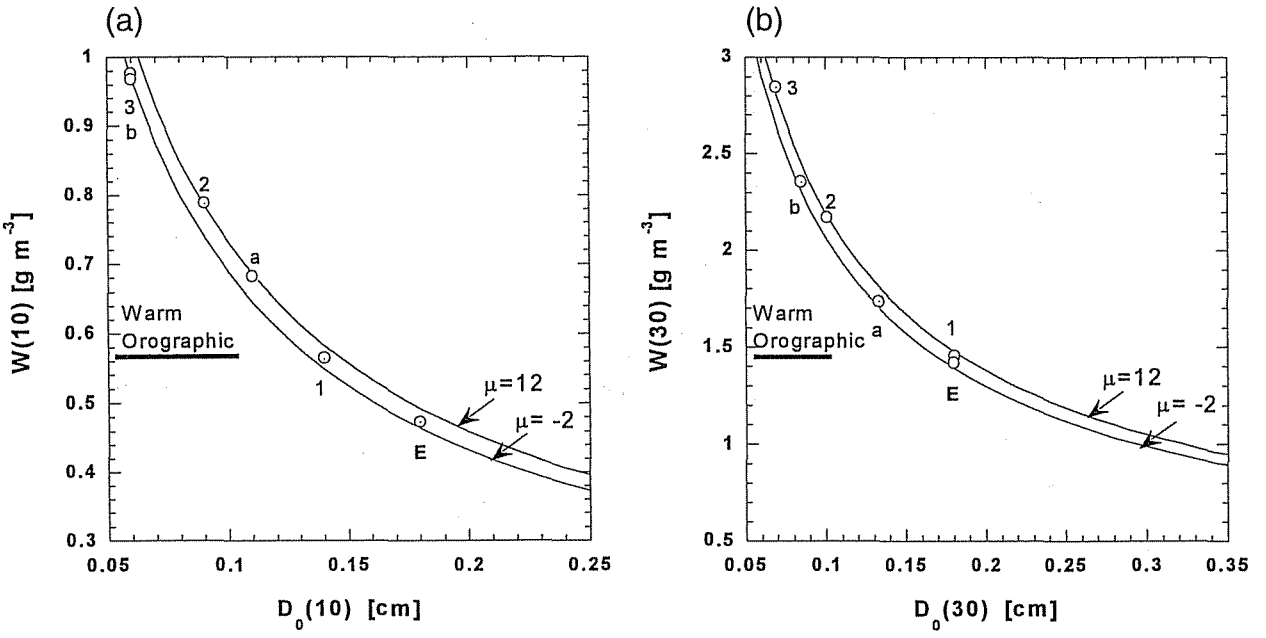

FIG. 10.11. (a) The liquid water content W vs median volume diameter D_0 for R = 10 mm h^{-1} from warm rain over orographic barriers. The labels of the points are according to Fig. 10.10 Other details are the same as Fig. 10.6a. (b) The liquid water content W vs median volume diameter D_0 for R = 30 mm h^{-1} from warm rain over orographic barriers. The labels of the points are according to Fig. 10.10. Note the systematic decrease of D_0 for increasing height. Other details are the same as in Fig. 10.6a.

of cloud droplets, both on water and ice hydrometeors; and (ii) "stratiform," where precipitation forms in updrafts <1 m s^{-1} mainly as ice crystals that aggregate into snowflakes and melt into rainfall in a radar "bright band;" and

c) orography, where low-level orographic lifting in clouds with active cloud drop coalescence can produce extremely small D_0 compared to all other types of rainfall and, hence, a gross radar underestimate of R.

Figures 10.12a,b illustrates that this classification orders

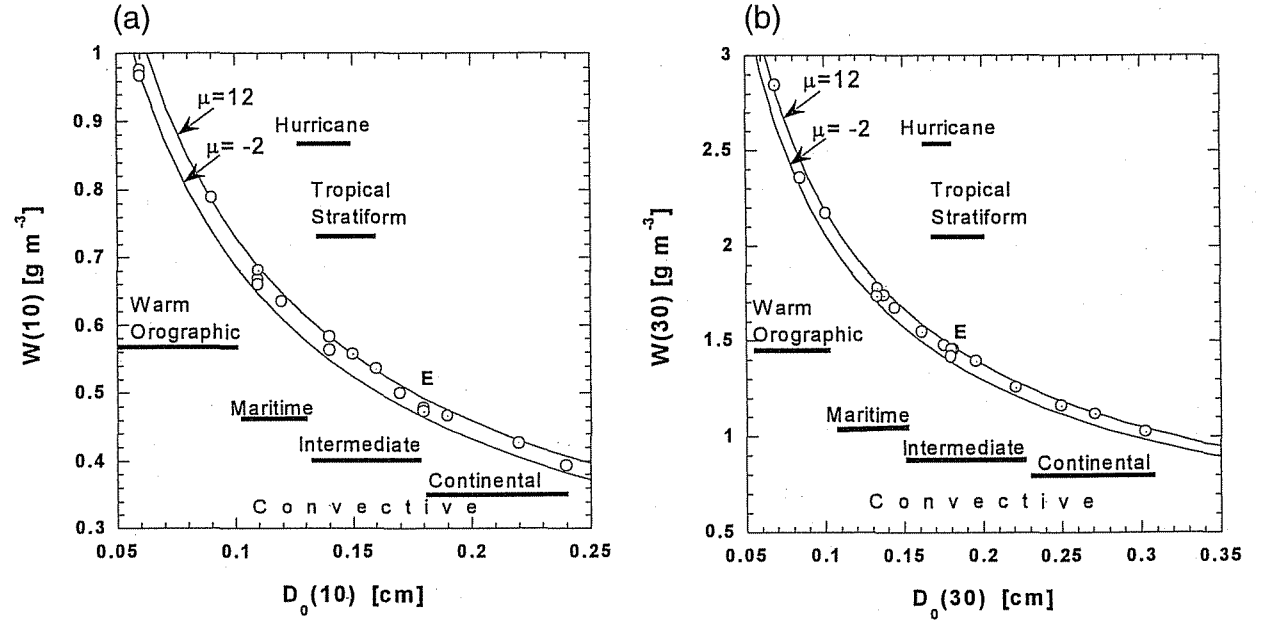

FIG. 10.12. (a) The liquid water content W for R = 10 mm h^{-1} for all the sampled rain types. The horizontal bars show the range of D_0 for the various rain types; E denotes the value of equilibrium RDSD. Other details are the same as in Fig. 10.6a. (b) The same as in (a) but for R = 30 mm h^{-1}.

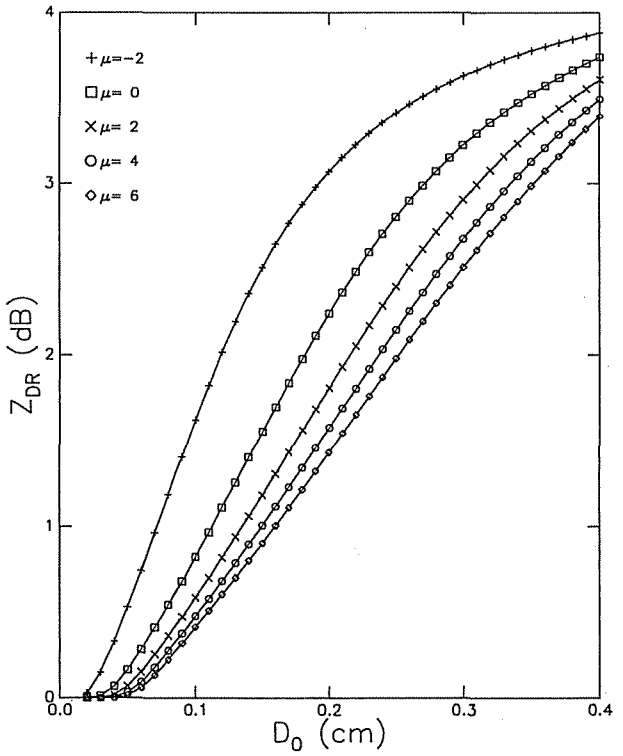

FIG. 10.13. The differential reflectivity factor Z_{DR} as a function of the median volume diameter D_0. The calculations assume that the axial ratio–diameter relation is that defined in Keenan et al. (2001) and that the raindrops are distributed according to a gamma distribution having shape parameter μ. Results are shown for values of μ = −2, 0, 2, 4, and 6. The radar wave length is assumed to be 10.7 cm and the maximum raindrop diameter D_{max} = 8 mm.

in a physically meaningful way the large range of variability of the Z–R and D_0. This classification scheme can explain a variability of R for a given Z by a factor of 1.5–2 for convective–stratiform classification, a factor of more than 3 for continental–maritime classification, and up to a factor of 10 in orographic precipitation.

The classification scheme reveals the potential for significant improvements in radar rainfall estimates by application of a dynamic Z–R relation, based on the microphysical, topographical, and dynamical context of the rain clouds while following known practices, such as

- determination of cloud microstructure by analyzing the dependence of the cloud drop effective radius on cloud-top temperature of growing convective elements, as done by Rosenfeld and Lensky (1998);
- determination of convective–stratiform separation from existence of bright band or from the horizontal structure of the reflectivity field (e.g., Churchill and Houze 1984);
- synoptic analysis of the low-level moisture orographic uplifting in clouds.

There are probably many more ways that can lead to this classification. This can serve as the foundation for a new generation of combined cloud physics–radar algorithms that will produce variable Z–R, which will hopefully lead to improvements in the rainfall measurements, not only when using reflectivity-only data, but also with polarimetric radars. The application of polarimetric radar data for the measurement of rainfall parameters and characterization of rainfall by type is covered in detail by Bringi and Chandrasekar (2001). In this work a discussion is presented only of the differential reflectivity technique. These radars possess the capability of acquiring simultaneous estimates of the two parameters of an exponential raindrop-size distribution through measurement of the backscattered reflectivity factors at horizontal and vertical polarization, Z_H and Z_V, respectively (Seliga and Bringi 1976). One of these parameters, the median volume diameter D_0, can be determined directly from the differential reflectivity Z_{DR}, defined as

$$Z_{DR} = 10 \log_{10}\left(\frac{Z_H}{Z_V}\right),$$

which is a function of only D_0, assuming that the RDSD is a function of only two parameters, as in the case of the exponential distribution, or, for the gamma distribution, that the shape of the RDSD is known. To illustrate the latter point, the differential reflectivity Z_{DR} is plotted in Fig. 10.13 versus D_0 for several values of the parameter μ in the gamma distribution. These results were calculated for a radar wavelength in the S band and assume that the maximum diameter of the RDSD is D_{max} = 8 mm. It is evident that for D_0 values as small as about 0.5 mm Z_{DR} has values at least as large as 0.2 dB. The latter value is considered to be well within the accuracy with which Z_{DR} can be measured so it may be concluded that it can be determined with high accuracy for all the situations discussed in this work. A method has been developed by Zhang et al. (2001) that enables polarimetric radar measurements to determine all three of the parameters of a gamma RDSD using only the reflectivity factor at horizontal polarization Z_{HH} and Z_{DR}. The method involves an empirical relation between μ and Λ and estimates raindrop median size with good accuracy, at least for storms in central Florida. It may therefore be concluded that Z_{DR} can be used as a means of classifying rainfall by type even for median volume diameters as small as 0.5 mm as in the case of orographic rainfall and even in the case where the RDSD shape is unknown. Another recent method for determination of the RDSD parameters N_0, D_m, and μ is described by Bringi et al. (2003). They show that these RDSD parameters change systematically between microphysically continental and maritime clouds along the same lines that were documented and physically explained in the current study.

Spaceborne radars, however, cannot employ dual-polarization measurements, because a falling drop remains perfectly round at the horizontal cross section regardless

of its size. Other radar methods, such as dual wavelength, will have to be developed for obtaining D_0. In the meantime, the classification by cloud microstructure, dynamical structure (convective–stratiform), and orographic component will have to play a major role in improving spaceborne rainfall measurements from satellites such as the Tropical Rainfall Measuring Mission.

Acknowledgments. A portion of the participation of CWU in this work was sponsored by Contract NAS 5-7782 with the National Aeronautics and Space Administration (NASA) Goddard Space Flight Center. DR's participation was funded by EURAINSAT, a shared-cost project (Contract EVG1-2000-00030) cofunded by the Research DG of the European Commission within the RTD activities of a generic nature of the Environment and Sustainable Development subprogram (5th Framework Programme).

REFERENCES

Atlas, D., 1955: The radar measurement of precipitation growth. Ph.D. thesis, Massachusetts Institute of Technology, 239 pp.

——, 1964: Advances in radar meteorology. *Advances in Geophysics,* Vol. 10, Academic Press, 317–478.

——, and A. C. Chmela, 1957: Physical–synoptic variations of drop-size parameters. *Proc. Sixth Weather Radar Conf.,* Cambridge, MA, Amer. Meteor. Soc., 21–29.

——, and C. W. Ulbrich, 1977: Path- and area-integrated rainfall measurement by microwave attenuation in the 1–3 cm band. *J. Appl. Meteor.,* **16,** 1322–1331.

——, and ——, 2000: An observationally based conceptual model of warm oceanic convective rain in the Tropics. *J. Appl. Meteor.,* **39,** 2165–2181.

——, ——, F. D. Marks Jr., E. Amitai, and C. R. Williams, 1999: Systematic variation of drop size and radar–rainfall relations. *J. Geophys. Res.,* **104,** 6155–6169.

——, ——, ——, R. A. Black, E. Amitai, P. T. Willis, and C. E. Samsury, 2000: Partitioning tropical oceanic and stratiform rains by draft strength. *J. Geophys. Res.,* **105,** 2259–2267.

Best, A. C., 1950: The size distribution of raindrops. *Quart. J. Roy. Meteor. Soc.,* **76,** 16–36.

Black, R. A., and J. Hallett, 1986: Observations of the distribution of ice in hurricanes. *J. Atmos. Sci.,* **43,** 802–822.

Blanchard, D. C., 1953: Raindrop size-distribution in Hawaiian rains. *J. Meteor.,* **10,** 457–473.

Bradley, S. G., and C. D. Stow, 1974: The measurement of charge and size of raindrops: Part II. Results and analysis at ground level. *J. Appl. Meteor.,* **13,** 131–147.

Bringi, V. N., and V. Chandrasekar, 2001: *Polarimetric Doppler Weather Radar.* Cambridge University Press, 636 pp.

——, ——, J. Hubbert, E. Gorgucci, W. L. Randeau, and M. Schoenhuber, 2003: Raindrop size distribution in different climatic regimes from disdrometer and dual-polarized radar analysis. *J. Atmos. Sci.,* **60,** 354–365.

Brown, P. S., Jr., 1989: Coalescence and breakup-induced oscillations in the evolution of the raindrop size distribution. *J. Atmos. Sci.,* **46,** 1186–1192.

Carbone, R. E., and L. D. Nelson, 1978: The evolution of raindrop spectra in warm-based convective storms as observed and numerically modeled. *J. Atmos. Sci.,* **35,** 2302–2314.

Cataneo, R., and G. E. Stout, 1968: Raindrop-size distributions in humid continental climates, and associated rainfall rate–radar reflectivity relationships. *J. Appl. Meteor.,* **7,** 901–907.

Caton, P. G. F., 1966: A study of raindrop size distributions in the free atmosphere. *Quart. J. Roy. Meteor. Soc.,* **92,** 15–30.

Chandrasekar, V., and V. N. Bringi, 1987: Simulation of radar reflectivity and surface measurements of rainfall. *J. Atmos. Oceanic Technol.,* **4,** 464–478.

——, R. Meneghini, and I. Zawadzki, 2003: Global and local precipitation measurements by radar. *Radar and Atmospheric Science: A Collection of Essays in Honor of David Atlas,Meteor. Monogr.,* No.52, Amer. Meteor. Soc., 215–236.

Churchill, D. D., and R. A. Houze Jr., 1984: Development and structure of winter monsoon cloud clusters on 10 December 1978. *J. Atmos. Sci.,* **41,** 933–960.

de Beauville, C. A., R. H. Petit, G. Marion, and J. P. Lacaux, 1988: Evolution of peaks in the spectral distribution of raindrops from warm isolated maritime clouds. *J. Atmos. Sci.,* **45,** 3320–3332.

Deirmendjian, D., 1969: *Electromagnetic Scattering on Spherical Polydispersions.* Elsevier, 290 pp.

Dingle, A. N., and K. R. Hardy, 1962: The description of rain by means of sequential rain-drop size distributions. *Quart. J. Roy. Meteor. Soc.,* **88,** 301–314.

Donaldson, N. R., 1984: Raindrop evolution with collisional breakup: Theory and models. Ph.D. thesis, University of Toronto, 181 pp.

Foote, G. B., 1966: A Z–R relation for mountain thunderstorms. *J. Appl. Meteor.,* **5,** 229–231.

Fujiwara, M., 1965: Raindrop-size distribution from individual storms. *J. Atmos. Sci.,* **22,** 585–591.

——, and T. Yanase, 1968: Raindrop Z–R relationships in different altitudes. *Proc. 13th Radar Meteorology Conf.,* Montreal, QC, Canada, Amer. Meteor. Soc., 380–383.

Haddad, Z. S., S. L. Durden, and E. Im, 1996: Parameterizing the raindrop size distribution. *J. Appl. Meteor.,* **35,** 3–13.

Houze, R. A., Jr., 1989: Observed structure of mesoscale convective systems and implications for large scale heating. *Quart. J. Roy. Meteor. Soc.,* **115,** 425–461.

Hu, Z., and R. Srivastava, 1995: Evolution of the raindrop size distribution by coalescence, breakup, and evaporation: Theory and observations. *J. Atmos. Sci.,* **52,** 1761–1783.

Huggel, A., W. Schmid, and A. Waldvogel, 1996: Raindrop size distributions and the radar bright band. *J. Appl. Meteor.,* **35,** 1688–1701.

Iguchi, T., T. Kozu, R. Meneghini, J. Awaka, and K. Okamoto, 2000: Rain-profiling algorithm for the TRMM precipitation radar. *J. Appl. Meteor.,* **39,** 2038–2052.

Imai, I., 1964: A fitting equation for raindrop-size distributions in various weather situations. *Proc. World Conf. on Radio Meteorology and 11th Weather Radar Conf.,* Boulder, CO, Amer. Meteor. Soc., 149A–149D.

Jorgensen, D. P., and P. T. Willis, 1982: A Z–R relationship for hurricanes. *J. Appl. Meteor.,* **21,** 356–366.

——, and M. A. LeMone, 1989: Vertical velocity characteristics of oceanic convection. *J. Atmos. Sci.,* **46,** 621–640.

Joss, J., and A. Waldvogel, 1970: A method to improve the accuracy of radar measured amounts of precipitation. Preprints, *14th Radar Meteorology Conf.,* Tucson, AZ, Amer. Meteor. Soc., 237–238.

——, and E. G. Gori, 1978: Shapes of raindrop size distributions. *J. Appl. Meteor.,* **17,** 1054–1061.

Keenan, T. D., L. D. Carey, D. S. Zrnic, and P. T. May, 2001: Sensitivity of 5-cm wavelength polarimetric radar variables to raindrop axial ratio and drop size distribution. *J. Appl. Meteor.,* **40,** 526–545.

Laws, J. O., and D. A. Parsons, 1943: The relation of raindrop-size to intensity. *Trans. Amer. Geophys. Union,* **24,** 452–460.

Levin, L. M., 1954: On the size distribution function for cloud droplets and rain drops. *Dokl. Akad. Nauk SSSR,* **94,** 1045–1053.

Levin, Z., G. Feingold, S. Tzivion, and A. Waldvogel, 1991: The evolution of raindrop spectra: Comparisons between modeled and observed spectra along a mountain slope in Switzerland. *J. Appl. Meteor.,* **30,** 893–900.

List, R., 1988: A linear radar reflectivity–rain-rate relationship for steady tropical rain. *J. Atmos. Sci.,* **45,** 3564–3572.

——, T. B. Low, N. Donaldson, E. Freire, and J. R. Gillespie, 1987:

Temporal evolution of drop spectra to collisional equilibrium in steady and pulsating rain. *J. Atmos. Sci.*, **44,** 362–372.

Maki, M., T. D. Keenan, Y. Sasaki, and K. Nakamura, 2001: Characteristics of the raindrop size distribution in tropical continental squall lines observed in Darwin, Australia. *J. Appl. Meteor.*, **40,** 1393–1412.

Markowitz, A. H., 1976: Raindrop size distribution expressions. *J. Appl. Meteor.*, **15,** 1029–1031.

Marshall, J. S., and W. McK. Palmer, 1948: The distribution of raindrops with size. *J. Meteor.*, **5,** 165–166.

——, R. C. Langille, and W. McK. Palmer, 1947: Measurement of rainfall by radar. *J. Meteor.*, **4,** 186–192.

Mueller, E. A., 1965: Radar rainfall studies. Ph.D. dissertation, University of Illinois at Urbana–Champaign, 89 pp.

——, and A. L. Sims, 1966: Radar cross sections from drop size spectra. Tech. Rep. ECOM-00032-F, Contract DA-28-043 AMC-00032(E), Illinois State Water Survey, Urbana, Illinois, 110 pp.

Orville, R. E., and R. W. Henderson, 1986: Global distribution of midnight lightning: September 1977 to August 1978. *Mon. Wea. Rev.*, **114,** 2640–2653.

Petrocchi, P. J., and K. J. Banis, 1980: Computer analysis of raindrop disdrometers' spectral data acquired during the 1979 SESAME project. Preprints, *19th Conf. on Radar Meteorology,* Miami Beach, FL, Amer. Meteor. Soc., 490–492.

Rogers, R. R., and R. J. Pilié, 1962: Radar measurements of drop size distribution. *J. Atmos. Sci.*, **19,** 503–506.

Rosenfeld, D., and I. M. Lensky, 1998: Spaceborne sensed insights into precipitation formation processes in continental and maritime clouds. *Bull. Amer. Meteor. Soc.*, **79,** 2457–2476.

Rutledge, S. A., E. R. Williams, and T. D. Keenan, 1992: The Down Under Doppler and Electricity Experiment (DUNDEE): Overview and preliminary results. *Bull. Amer. Meteor. Soc.*, **73,** 3–16.

Sauvageot, H., 1994: Rainfall measurement by radar: A review. *Atmos. Res.*, **35,** 27–54.

——, and J.-P. Lacaux, 1995: The shape of averaged drop size distributions. *J. Atmos. Sci.*, **52,** 1070–1083.

Seliga, T. A., and V. N. Bringi, 1976: Potential use of radar differential reflectivity measurements at orthogonal polarizations for measuring precipitation. *J. Appl. Meteor.*, **15,** 69–76.

Sims, A. L., 1964: Case studies of the areal variations in raindrop size distributions. *Proc. World Conf. on Radio Meteorology and 11th Weather Radar Conf.*, Boulder, CO, Amer. Meteor. Soc., 162–165.

Srivastava, R. C., 1971: Size distribution of raindrops generated by their breakup and coalescence. *J. Atmos. Sci.*, **28,** 410–415.

Steiner, M., and A. Waldvogel, 1987: Peaks in raindrop size distributions. *J. Atmos. Sci.*, **44,** 3127–3133.

Stewart, R. E., J. D. Marwitz, J. C. Pace, and R. E. Carbone, 1984: Characteristics through the melting layer of stratiform clouds. *J. Atmos. Sci.*, **41,** 3227–3237.

Stout, G. E., and E. A. Mueller, 1968: Survey of relationships between rainfall rate and radar reflectivity in the measurement of precipitation. *J. Appl. Meteor.*, **7,** 465–474.

Testud, J., S. Oury, R. A. Black, P. Amayenc, and X. Dou, 2001: The concept of "normalized" distributions to describe raindrop spectra: A tool for cloud physics and cloud remote sensing. *J. Appl. Meteor.*, **40,** 1118–1140.

Tokay, A., and D. A. Short, 1996: Evidence from tropical raindrop spectra of the origin of rain from stratiform and convective clouds. *J. Appl. Meteor.*, **35,** 355–371.

——, ——, and B. Fisher, 1995: Convective vs. stratiform precipitation classification from surface measured drop size distributions at Darwin, Australia and Kapingamarangi atoll. Preprints, *27th Conf. on Radar Meteorology,* Vail, CO, Amer. Meteor. Soc., 690–693.

Ulbrich, C. W., 1983: Natural variations in the analytical form of the raindrop size distribution. *J. Climate Appl. Meteor.*, **22,** 1764–1775.

——, 1985: The effects of drop size distribution truncation on rainfall integral parameters and empirical relations. *J. Climate Appl. Meteor.*, **24,** 580–590.

——, 1992: Effects of drop size distribution truncation on computer simulations of dual-measurement radar methods. *J. Appl. Meteor.*, **31,** 689–699.

——, 1993: Corrections to empirical relations derived from rainfall disdrometer data for effects due to drop size distribution truncation. *Atmos. Res.*, **34,** 207–215.

——, and D. Atlas, 1978: The rain parameter diagram: Methods and applications. *J. Geophys. Res.*, **83C** 1319–1325.

——, and ——, 1998: Rainfall microphysics and radar properties: Analysis methods for drop size spectra. *J. Appl. Meteor.*, **37,** 912–923.

——, and ——, 2002: On the separation of tropical convective and stratiform rains. *J. Appl. Meteor.*, **41,** 188–195.

——, M. Petitdidier, and E. F. Campos, 1999: Radar properties of tropical rain found from disdrometer data at Arecibo, PR. Preprints, *29th Int. Conf. on Radar Meteorology,* Montreal, QC, Canada, Amer. Meteor. Soc., 676–679.

Valdez, M. P., and K. C. Young, 1985: Number fluxes in equilibrium raindrop populations: A Markov chain analysis. *J. Atmos. Sci.*, **42,** 1024–1036.

Waldvogel, A., 1974: The N_0 jump of raindrop spectra. *J. Atmos. Sci.*, **31,** 1067–1078.

Williams, E. R., S. A. Rutledge, S. G. Geotis, N. Renno, E. Rasmussen, and T. Rickenbach, 1992: A radar and electrical study of tropical "hot towers." *J. Atmos. Sci.*, **49,** 1386–1395.

——, and Coauthors, 2002: Contrasting convective regimes over the Amazon: Implications for cloud electrification. *J. Geophys. Res.*, **107,** doi:10.1029/2001ID000380.

Willis, P. T., 1984: Functional fits to some observed drop size distributions and parameterization of rain. *J. Atmos. Sci.*, **41,** 1648–1661.

Wilson, J. W., and E. A. Brandes, 1979: Radar measurement of rainfall—A summary. *Bull. Amer. Meteor. Soc.*, **60,** 1048–1058.

Zawadzki, I., and M. de Agostinho Antonio, 1988: Equilibrium raindrop size distributions in tropical rain. *J. Atmos. Sci.*, **45,** 3452–3459.

Zhang, G., J. Vivekanandan, and E. Brandes, 2001: A method for estimating rain rate and drop size distribution from polarimetric radar measurements. *IEEE Trans. Geosci. Remote Sens.*, **39,** 830–841.

Zipser, E. J., 1994: Deep cumulonimbus cloud systems in the Tropics with and without lightning. *Mon. Wea. Rev.*, **122,** 1837–1851.

——, and M. A. LeMone, 1980: Cumulonimbus vertical velocity events in GATE. Part II: Synthesis and model core structure. *J. Atmos. Sci.*, **37,** 2458–2469.

——, and K. Lutz, 1994: The vertical profile of radar reflectivity of convective cells: A strong indicator of storm intensity and lightning probability. *Mon. Wea. Rev.*, **122,** 1751–1759.